Signal Transmission Using Underwater Acoustic Vector Transducers

C. Chen and A. Abdi, *Senior Member, IEEE*

***Abstract* — Recent studies show that a vector transducer which measures signal in acoustic particle velocity channels can serve as a compact multichannel communication receiver. In this paper, data transmission via underwater particle velocity channels using a vector transducer is investigated. System and channel equations are derived and a method for signal modulation in particle velocity channels is proposed. The signal is transmitted with opposite polarities, which makes the received signal the convolution of the transmitted signal and a particle velocity channel response. System performance analysis demonstrates the feasibility and advantages of data transmission using a vector transducer.**

I. Introduction

Vector transducers are devices that measure or excite the vector components of the acoustic field such as acoustic particle velocity. They have been extensively used for source localization, beamforming and direction finding [1]-[9]. A vector transducer equalizer is proposed in [10] as a multichannel communication receiver. Possible channel correlations in a vector transducer receiver are studied in [11], and delay and Doppler spreads of particle velocity channels are investigated in [12]. Data reception and equalization via underwater acoustic communication experiments have demonstrated the usefulness of vector transducers as compact multichannel receivers [13]. In this paper data transmission using a vector transducer is investigated. It is well known that particle velocity is the spatial gradient of the acoustic pressure field [14]. On the other hand, a dipole composed of two closely-spaced scalar transducers is a vector transducer that can measure particle velocity [14]. By modulating the signal on a dipole in a certain way proposed in the paper, the received signal becomes the convolution of the transmit signal with particle velocity channels. This can be considered as modulation in particle velocity channels. Therefore, as shown in this paper, one can use a vector transducer as a small multichannel transmitter, to achieve transmit diversity and improve system performance, by modulating the data over the vector and scalar components

C. Chen and A. Abdi are with the Center for Wireless Communication and Signal Processing Research, Department of Electrical and Computer Engineering, New Jersey Institute of Technology, Newark, NJ 07102, USA.
This work is supported in part by the National Science Foundation (NSF), Grant CCF-0830190.

of the acoustic field. To demonstrate this, channel modeling aspects of vector transducer-based communication systems are investigated in this paper, as well as signal modulation and system performance analysis.

To explain the basic concepts, in Section II first a system with a dipole transmitter and a vector transducer receiver is developed. Then it is extended to a system with a vector transducer at the transmit side. Some characteristics of the channels encountered in the proposed system are investigated in Section III, whereas Section IV includes analytical and simulation-based system performance results. Concluding remarks are given in Section V, and proofs and detailed derivations are provided in appendices.

Notation: we use j for $\sqrt{-1}$, $E[\cdot]$ for mathematical expectation, ^{T} for transpose, * for complex conjugate, † for complex conjugate transpose, $\oplus$ for convolution, $\otimes$ for Kronecker product and $\delta(\cdot)$ for the Dirac delta function.

II. Signals and Channels in the Proposed System

In the two-dimensional *y*-*z* (range-depth) plane, a vector transducer measures or stimulates three components of the acoustic field: pressure as well as y and z components of the particle velocity. A scalar transducer deals with the acoustic pressure. The *y* and *z* components of acoustic particle velocity, on the other hand, can be measured or stimulated by two dipoles in *y* and *z* directions, respectively. This is because particle velocity in a certain direction is the spatial derivative of the acoustic field in that direction. In Fig. 1 there is one vector transducer at the transmit side and one vector transducer at the receive side, where each consists of three scalar transducers. The three scalar transducers at the *Tx* are labeled as 1, 2 and 3, with the scalar pairs {2, 3} and {2, 1} acting as two dipoles in *y* and *z* directions, respectively. At the *Rx*, there are two dipoles in *y* and *z* directions as well. They measure the *y* and *z* components of the acoustic particle velocity at the point (y_0, z_0), whereas scalar transducer #2 measures the acoustic pressure at (y_0, z_0). Overall there are nine pressure channels in Fig.1, where p_{iq} stands for the channel from the scalar transducer *i* at *Tx* to the scalar transducer *q* at *Rx*, $i = 1,2,3$ and $q = 1,2,3$. A list of all the channels defined and used in the paper is provided in Table I.

According to the linearized equation for plane waves [14] at frequency f_0, for each transducer at *Tx* we define two particle velocity channels at *Rx* at (y_0, z_0). More specifically, for Tx_1 there are $v_z^{Tx_1}$ and $v_y^{Tx_1}$, for Tx_2 we have $v_z^{Tx_2}$ and $v_y^{Tx_2}$ and finally for Tx_3 we have $v_z^{Tx_3}$ and $v_y^{Tx_3}$. These six channels are defined by the following equations in (1), with $L_{Rx} \to 0$, based on the fact that velocity is the spatial derivative of the pressure.

$$
\begin{aligned}
v_z^{Tx_1} &= -(j\rho_0\omega_0)^{-1}(p_{11}-p_{12})/L_{Rx},\ \ v_y^{Tx_1} = -(j\rho_0\omega_0)^{-1}(p_{13}-p_{12})/L_{Rx},\\
v_z^{Tx_2} &= -(j\rho_0\omega_0)^{-1}(p_{21}-p_{22})/L_{Rx},\ \ v_y^{Tx_2} = -(j\rho_0\omega_0)^{-1}(p_{23}-p_{22})/L_{Rx},\\
v_z^{Tx_3} &= -(j\rho_0\omega_0)^{-1}(p_{31}-p_{32})/L_{Rx},\ \ v_y^{Tx_3} = -(j\rho_0\omega_0)^{-1}(p_{33}-p_{32})/L_{Rx}.
\end{aligned}
\tag{1}
$$

Here ρ_0 is the fluid density, $\omega_0 = 2\pi f_0$ and L_{Rx} is the small spacing between the transducers at the *Rx* side.

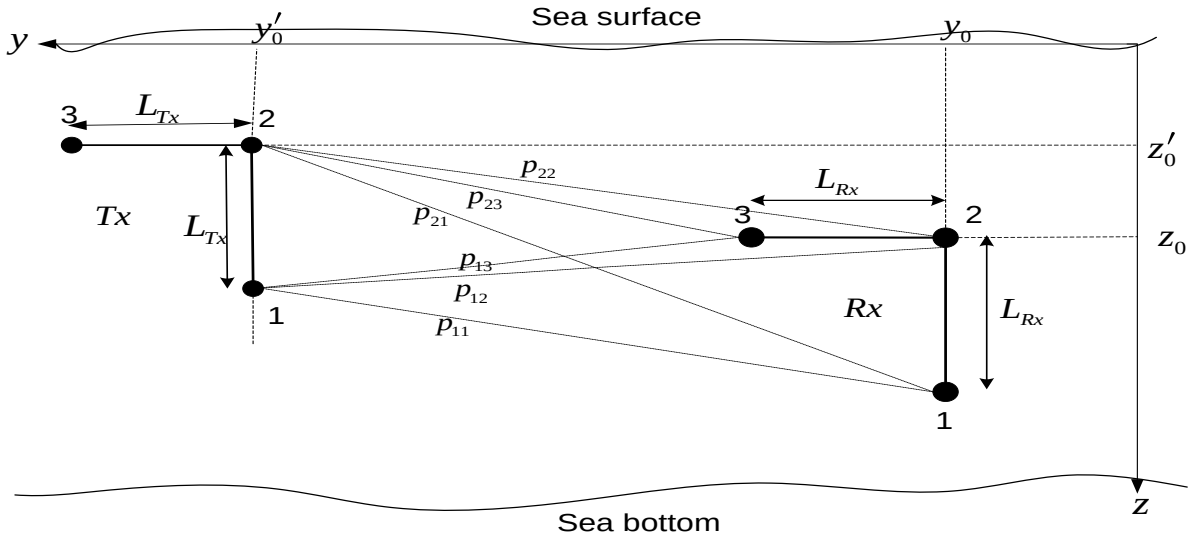

Fig. 1. The proposed vector transducer underwater acoustic communication system. There is one vector transmitter and one vector receiver. Pressure channels from the third transducer are not shown, to keep the figure easy to read.

A. Single Dipole Transmitter

To modulate a signal on the *z* velocity channel, we use the vertical dipole at the *Tx* side in Fig. 1. More specifically, to transmit the symbol *s*, we modulate $s/(jkL_{Tx})$ and $-s/(jkL_{Tx})$ on Tx_1 and Tx_2, respectively, where L_{Tx} denotes the spacing between the two transmit scalar transducers, $k = 2\pi/\lambda$ is the wavenumber and λ is the wavelength. Since *z* velocity is the spatial gradient of the pressure field in the z direction, this transmission scheme means that the symbol *s* is modulated on the z velocity channel. This can be better understood by writing the equation for the received signal at each scalar transducer at the *Rx* side

$$
r_1 = ((p_{11}-p_{21})/(jkL_{Tx})) \oplus s,\quad r_2 = ((p_{12}-p_{22})/(jkL_{Tx})) \oplus s,\quad r_3 = ((p_{13}-p_{23})/(jkL_{Tx})) \oplus s. \tag{2}
$$

As proved in Appendix I for small L_{Tx}, each channel $(p_{1q}-p_{2q})/(jkL_{Tx})$ in (2), $q = 1,2,3$, is a *pressure-equivalent z* velocity channel with which the symbol *s* is convolved and measured at the point *q*. Note that $(p_{1q}-p_{2q})/L_{Tx}$ is the *z* velocity, i.e., the spatial gradient of the pressure. Upon normalizing it by the scaling factor *jk* it becomes *pressure-equivalent z* velocity. This way all the channels in the proposed system have the same pressure unit.

The *z* and *y* particle velocity signals at *Rx* are spatial gradients of the received signals r_1, r_2, and r_3, measured by the two receive dipoles as $L_{Rx} \to 0$

$$\eta_z = -(j\rho_0\omega_0)^{-1}(r_1 - r_2)/L_{Rx}, \quad \eta_y = -(j\rho_0\omega_0)^{-1}(r_3 - r_2)/L_{Rx}. \tag{3}$$

By combining (1), (2) and (3), the *z* and *y* velocity components at *Rx* can be written as

$$\eta_z = ((v_z^{Tx_1} - v_z^{Tx_2})/(jkL_{Tx})) \oplus s, \quad \eta_y = ((v_y^{Tx_1} - v_y^{Tx_2})/(jkL_{Tx})) \oplus s. \tag{4}$$

Now we convert velocity channels and signals to *pressure-equivalent* quantities. Corresponding to the six particle velocity channels in (1), there are six pressure-equivalent particle velocity channels $p_z^{Tx_1}$, $p_z^{Tx_2}$, $p_z^{Tx_3}$, $p_y^{Tx_1}$, $p_y^{Tx_2}$ and $p_y^{Tx_3}$, obtained by multiplying (1) by the negative of the acoustic impedance $-\rho_0 c$ [10] and using the fact that $\omega_0 = ck$, with *c* as the sound speed

$$\begin{aligned}
p_z^{Tx_1} &= -\rho_0 c v_z^{Tx_1} = (jk)^{-1}(p_{11} - p_{12})/L_{Rx}, \quad p_y^{Tx_1} = -\rho_0 c v_y^{Tx_1} = (jk)^{-1}(p_{13} - p_{12})/L_{Rx}, \\
p_z^{Tx_2} &= -\rho_0 c v_z^{Tx_2} = (jk)^{-1}(p_{21} - p_{22})/L_{Rx}, \quad p_y^{Tx_2} = -\rho_0 c v_y^{Tx_2} = (jk)^{-1}(p_{23} - p_{22})/L_{Rx}, \\
p_z^{Tx_3} &= -\rho_0 c v_z^{Tx_3} = (jk)^{-1}(p_{31} - p_{32})/L_{Rx}, \quad p_y^{Tx_3} = -\rho_0 c v_y^{Tx_3} = (jk)^{-1}(p_{33} - p_{32})/L_{Rx}.
\end{aligned} \tag{5}$$

Similarly, the pressure-equivalent *z* and *y* velocity signals at *Rx* are η_z and η_y multiplied by $-\rho_0 c$

$$r_z = -\rho_0 c \eta_z, \quad r_y = -\rho_0 c \eta_y. \tag{6}$$

By substituting (4) into (6) and upon using the channel definitions in (5) we obtain

$$r_z = ((p_z^{Tx_1} - p_z^{Tx_2})/(jkL_{Tx})) \oplus s, \quad r_y = ((p_y^{Tx_1} - p_y^{Tx_2})/(jkL_{Tx})) \oplus s. \tag{7}$$

To include the effect of noise, pressure-equivalent ambient velocity noise terms ξ_z and ξ_y should be added to (7), whereas the ambient pressure noise ξ_2 needs to be added to the middle equation in (2). The final set of noisy signals received at *Rx* is given by

$$r_2 = p^z \oplus s + \xi_2, \quad r_y = p_y^z \oplus s + \xi_y, \quad r_z = p_z^z \oplus s + \xi_z, \tag{8}$$

where $p^z = (jk)^{-1}(p_{12} - p_{22})/L_{Tx}$, $p_y^z = (jk)^{-1}(p_y^{Tx_1} - p_y^{Tx_2})/L_{Tx}$ and $p_z^z = (jk)^{-1}(p_z^{Tx_1} - p_z^{Tx_2})/L_{Tx}$ are pressure-equivalent impulse responses of the three channels in the system. Note that the superscript *z* indicates that the transmitter is a dipole in the *z* direction, whereas the subscripts *y* and *z* mean that a horizontal and a vertical dipole are used at the *Rx* side, respectively.

B. Vector Transmitter

Now we extend the vertical dipole transmitter to a vector transmitter which includes two dipoles in *z* and *y* directions using the following method, three data streams can be modulated on the pressure, *z*-velocity and *y*-velocity channels. Let the symbols modulated on the three scalar transducers 1, 2 and 3 at *Tx* be $s_1 + s_2/(jkL_{Tx})$, $s_3/(kL_{Tx}) - s_2/(jkL_{Tx})$ and $-s_3/(kL_{Tx})$, respectively. Since velocity is the spatial

gradient of the pressure, one can intuitively see that symbol s_1 is sent via the pressure channel, whereas symbols s_2 and s_3 are transmitted via the *z* and *y* acoustic velocity channels, respectively.

TABLE I
A LIST OF CHANNELS AND THEIR PARAMETERS

p_{iq}	Pressure channel response from the transducer *i* at *Tx* to the transducer *q* at *Rx*, $i=1,2,3$ and $q=1,2,3$
$v_z^{Tx_i}$ and $v_y^{Tx_i}$	Vertical and horizontal components of particle velocity channels from Tx_i to *Rx*, $i=1,2,3$
$p_z^{Tx_i}$ and $p_y^{Tx_i}$	Vertical and horizontal components of pressure-equivalent particle velocity channels from Tx_i to *Rx*, $i=1,2,3$
p^d, p_z^d, p_y^d	Pressure, as well as vertical and horizontal components of pressure-equivalent particle velocity channels from a transmit dipole to Rx_2, *d=z* indicates a vertical transmit dipole and *d=y* means a horizontal transmit dipole
$p_{Rx_q}^d$	Pressure channel response from a dipole transmitter to the receive scalar transducer *q*, $q=1,2,3$ and *d=z,y*
Ω^d, Ω_y^d, Ω_z^d	Powers of the channels p^d, p_y^d and p_z^d, *d=z,y*
Ω^p, Ω_y^p, Ω_z^p	Powers of the channels p_{12}, $p_y^{Tx_1}$ and $p_z^{Tx_1}$
ρ_y^d, ρ_z^d, ρ_{zy}^d	Correlations among the channel pairs $\{p^d, p_y^d\}$, $\{p^d, p_z^d\}$ and $\{p_y^d, p_z^d\}$, *d=z,y*
ρ^y, ρ^z, ρ^{zy}	Correlations among the channel pairs $\{p^y, p_{12}\}$, $\{p^z, p_{12}\}$ and $\{p^z, p^y\}$
ρ_{12}, ρ_{13}, ρ_{23}	Correlations among the channel pairs $\{p_{12}, p_{22}\}$, $\{p_{12}, p_{32}\}$ and $\{p_{22}, p_{32}\}$

To show this analytically, similarly to (2) we write the received signal of each scalar transducer at *Rx*

$$\begin{aligned} r_1 &= p_{11} \oplus s_1 + ((p_{11}-p_{21})/(jkL_{Tx})) \oplus s_2 - ((p_{31}-p_{21})/(kL_{Tx})) \oplus s_3, \\ r_2 &= p_{12} \oplus s_1 + ((p_{12}-p_{22})/(jkL_{Tx})) \oplus s_2 - ((p_{32}-p_{22})/(kL_{Tx})) \oplus s_3, \\ r_3 &= p_{13} \oplus s_1 + ((p_{13}-p_{23})/(jkL_{Tx})) \oplus s_2 - ((p_{33}-p_{23})/(kL_{Tx})) \oplus s_3. \end{aligned} \tag{9}$$

By combining the channels $p_z^{Tx_i}$ and $p_y^{Tx_i}$ from (5) with (9), $i=1,2,3$, the received *z*-velocity and *y*-velocity signals at *Rx* can be written as

$$\begin{aligned} r_z &= (r_1-r_2)/(jkL_{Rx}) = p_z^{Tx_1} \oplus s_1 + ((p_z^{Tx_1}-p_z^{Tx_2})/(jkL_{Tx})) \oplus s_2 - ((p_z^{Tx_3}-p_z^{Tx_2})/(kL_{Tx})) \oplus s_3, \\ r_y &= (r_3-r_2)/(jkL_{Rx}) = p_y^{Tx_1} \oplus s_1 + ((p_y^{Tx_1}-p_y^{Tx_2})/(jkL_{Tx})) \oplus s_2 - ((p_y^{Tx_3}-p_y^{Tx_2})/(kL_{Tx})) \oplus s_3. \end{aligned} \tag{10}$$

Upon including the noise terms, the received pressure, *y*-velocity and *z*-velocity signals, respectively, can be written as

$$\begin{aligned} r_2 &= p_{12} \oplus s_1 + p^z \oplus s_2 - jp^y \oplus s_3 + \xi_2, \\ r_y &= p_y^{Tx_1} \oplus s_1 + p_y^z \oplus s_2 - jp_y^y \oplus s_3 + \xi_y, \\ r_z &= p_z^{Tx_1} \oplus s_1 + p_z^z \oplus s_2 - jp_z^y \oplus s_3 + \xi_z. \end{aligned} \tag{11}$$

The three new channels in (11) are defined as $p^y=(jk)^{-1}(p_{32}-p_{22})/L_{Tx}$, $p_y^y=(jk)^{-1}(p_y^{Tx_3}-p_y^{Tx_2})/L_{Tx}$ and $p_z^y=(jk)^{-1}(p_z^{Tx_3}-p_z^{Tx_2})/L_{Tx}$. They represent the three pressure-equivalent impulse responses from the *y*-oriented dipole at *Tx* to the *Rx* in the system.

III. Channel Transfer Functions in the Vector System

A channel model for a vector communication receiver is developed in [11], where the channel transfer functions for a system composed of a scalar transducer at the transmit side and a vector transducer at the receive side are derived [11]. However, channel transfer functions in systems where both the transmitter and receiver are equipped with vector transducers are unknown. In this section we derive time-invariant wideband channel transfer functions from a vector transducer transmitter to a vector transducer receiver. They will be used in the next section for system performance analysis.

In this paper, we consider an important underwater acoustic communication channel, i.e., the shallow water, which is a multipath channel due to the multiple interactions of acoustic waves with the sea boundaries. Shallow waters are bounded by the sea surface and the sea bottom. When the sea boundaries are relatively smooth, channel transfer functions consist of the direct ray and multiple rays reflected from the boundaries. On the other hand, when the sea boundaries are rough, channel transfer functions are composed of scattered rays from the boundaries. We discuss these two different cases in Subsections III.A and III.B, respectively. The results will be used in the next section for system performance assessment.

A. Geometrical Multipath Channel Transfer Functions

A model for the acoustic pressure channel transfer function in shallow waters with smooth boundaries can be found in [15] and [16], where reflections from the bottom and surface are the dominant propagation mechanisms. This model is based on the acoustic rays traveled from the scalar transmitter to the scalar receiver, and the pressure channel transfer function is obtained by adding up the rays at the receive side. The model has been used by many authors for simulating shallow waters to study the performance of a variety of underwater communication systems. See, for example, [17] [18] [19] [20]. It is also extended to systems with multiple transmit and receive scalar transducers [21]. In what follows we extend this model to derive channel transfer functions from a transmit vector transducer to a receive vector transducer in shallow waters, where an isovelocity profile is assumed.

In shallow underwater acoustic communication channels, a ray from transmitter may experience a few times of bounces between the sea surface and bottom before it reaches the receiver. According to the first bounce after leaving the transmitter and the last bounce before arriving the receiver, rays can be classified into four groups [15][16]. As shown in Fig.2, these four groups are: first bounce at surface, last bounce at bottom (*SB*), first bounce at bottom, last bounce at bottom (*BB*), first bounce at surface, last bounce at surface (*SS*), and first bounce at bottom, last bounce at surface (*BS*). When the Rayleigh parameter is much

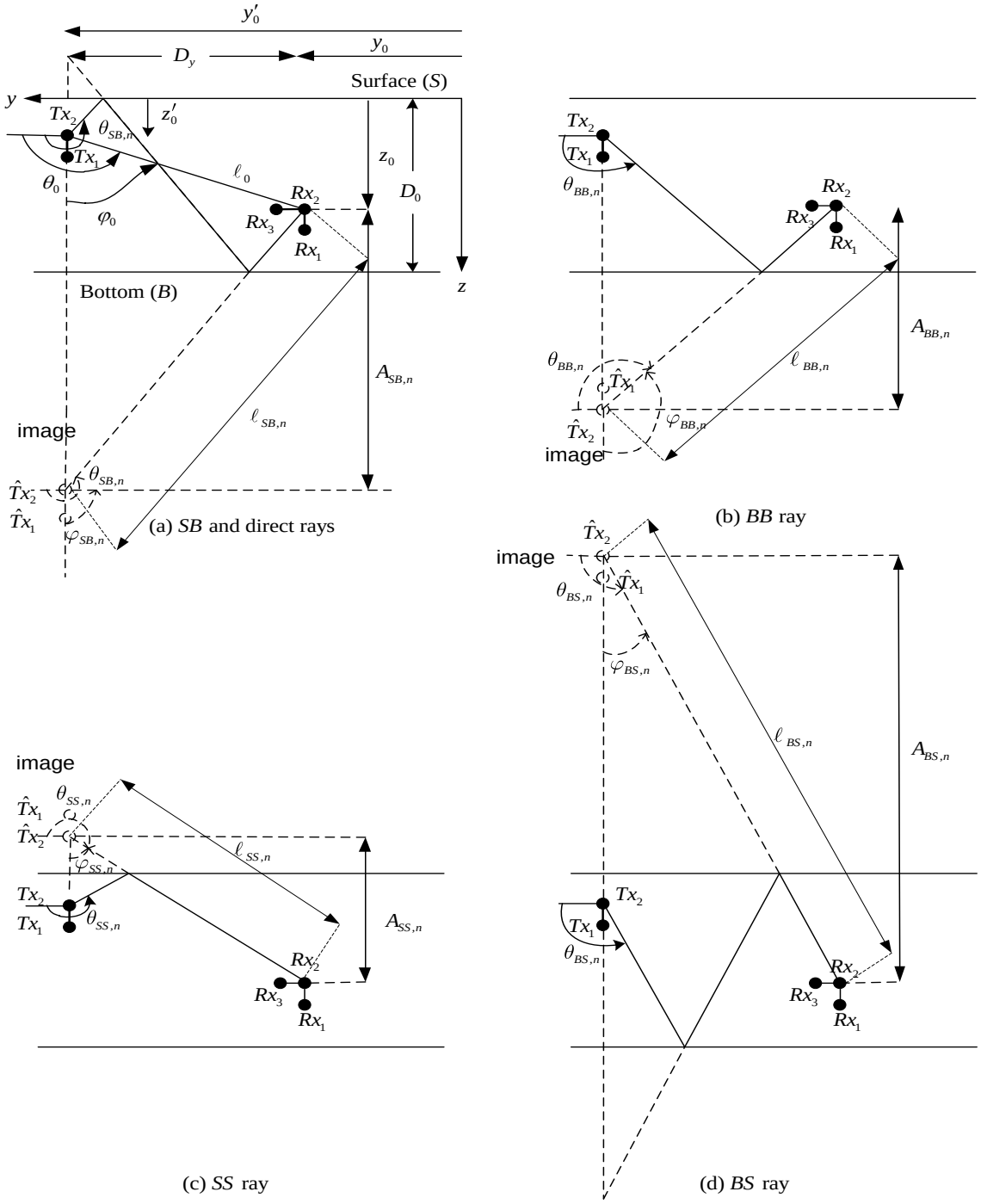

Fig. 2. Four groups of rays in a shallow water multipath channel.

less than unity, boundaries act like reflectors with coherent specular reflection [22]. Let the water depth be a constant value D_0 and D_y be the transmission range, such that $D_y / D_0 \gg 2n+1$ in the shallow water channel, where $n = 1, 2, \cdots\cdots$ numerates different paths from the transmitter to the receiver. For a ray from the transmitter Tx_2 at (y_0', z_0') to the receiver Rx_2 at (y_0, z_0) in Fig.2, the path length is $\ell_{XW,n} = \sqrt{D_y^{\,2} + A_{XW,n}^2}$ [15] [16], with $A_{XW,n}$ as the vertical projection of $\ell_{XW,n}$ for the *n*-th ray from the *XW*

group, where $X, W = S$ or B. The combined pressure loss for the *n*-th ray in each group, $R_{XW,n}$, is due to multiple surface and bottom reflections, where the complex surface reflection coefficient is denoted as β and the bottom reflection coefficient is considered to be unity and negative[16]. Similarly to [16], the analysis assumes β to be real-valued and negative. For the *n*-th path from Tx_2 to Rx_2, the angle of departure (AOD) $\theta_{XW,n}$ is measured with respect to the positive *y* axis in Fig. 2, counterclockwise. Let us define the path length and AOD for the direct path from Tx_2 to Rx_2 as $\ell_0 = \sqrt{A_0^2 + D_y^2}$ and $\theta_0 = \pi - \arctan(A_0 / D_y)$, respectively, where $A_0 = z_0 - z_0'$. Equations for ℓ's, *R*'s and θ's are provided in Appendix II. Also let N_{XW}'s be the number of rays in each group. As shown in Fig. 2, each reflected ray from the dipole at the transmit side to the receiver can be represented by a direct ray from the image of the dipole at the transmit side to the receiver. Using the direct ray expressions derived in Appendix I, it is shown in Appendix II that the baseband pressure-equivalent channel transfer function from the dipole at the transmit side to the vector transducer receiver can be written as the superposition of rays and their images. For example, $P^z(f)$, the channel transfer function from the vertical dipole to the point Rx_2 can be written as (12) . Expressions for the baseband pressure-equivalent channel transfer functions measured by a receive vertical dipole and a receive horizontal dipole, $P_z^z(f)$ and $P_y^z(f)$, respectively, are also derived in Appendix II and provided in (13) and (14) . Channel transfer functions from a horizontal transmit dipole are given in (54)-(56) in Appendix II as well.

$$
\begin{aligned}
P^z(f) = {} & \sin(\theta_0)\exp(-jk\ell_0)\exp(-j\omega\ell_0/c)/\ell_0 \\
& + \sum_{n_1=1}^{N_{SB}} R_{SB,n_1}\sin(\theta_{SB,n_1})\exp(-jk\ell_{SB,n_1})\exp(-j\omega\ell_{SB,n_1}/c)/\ell_{SB,n_1} \\
& + \sum_{n_2=1}^{N_{BB}} R_{BB,n_2}\sin(\theta_{BB,n_2})\exp(-jk\ell_{BB,n_2})\exp(-j\omega\ell_{BB,n_2}/c)/\ell_{BB,n_2} \\
& + \sum_{n_3=1}^{N_{SS}} R_{SS,n_3}\sin(\theta_{SS,n_3})\exp(-jk\ell_{SS,n_3})\exp(-j\omega\ell_{SS,n_3}/c)/\ell_{SS,n_3} \\
& + \sum_{n_4=1}^{N_{BS}} R_{BS,n_4}\sin(\theta_{BS,n_4})\exp(-jk\ell_{BS,n_4})\exp(-j\omega\ell_{BS,n_4}/c)/\ell_{BS,n_4}.
\end{aligned}
\tag{12}
$$

$$
\begin{aligned}
P_z^z(f) = {} & -\sin^2(\theta_0)\exp(-jk\ell_0)\exp(-j\omega\ell_0/c)/\ell_0 \\
& - \sum_{n_1=1}^{N_{SB}} R_{SB,n_1}\sin^2(\theta_{SB,n_1})\exp(-jk\ell_{SB,n_1})\exp(-j\omega\ell_{SB,n_1}/c)/\ell_{SB,n_1} \\
& + \sum_{n_2=1}^{N_{BB}} R_{BB,n_2}\sin^2(\theta_{BB,n_2})\exp(-jk\ell_{BB,n_2})\exp(-j\omega\ell_{BB,n_2}/c)/\ell_{BB,n_2} \\
& + \sum_{n_3=1}^{N_{SS}} R_{SS,n_3}\sin^2(\theta_{SS,n_3})\exp(-jk\ell_{SS,n_3})\exp(-j\omega\ell_{SS,n_3}/c)/\ell_{SS,n_3} \\
& - \sum_{n_4=1}^{N_{BS}} R_{BS,n_4}\sin^2(\theta_{BS,n_4})\exp(-jk\ell_{BS,n_4})\exp(-j\omega\ell_{BS,n_4}/c)/\ell_{BS,n_4}.
\end{aligned}
\tag{13}
$$

$$P_y^z(f)=-\sin(\theta_0)\cos(\theta_0)\exp(-jk\ell_0)\exp(-j\omega\ell_0/c)/\ell_0-\sum_{n_1=1}^{N_{SB}}R_{SB,n_1}\sin(\theta_{SB,n_1})\cos(\theta_{SB,n_1})\exp(-jk\ell_{SB,n_1})\exp(-j\omega\ell_{SB,n_1}/c)/\ell_{SB,n_1}$$
$$-\sum_{n_2=1}^{N_{BB}}R_{BB,n_2}\sin(\theta_{BB,n_2})\cos(\theta_{BB,n_2})\exp(-jk\ell_{BB,n_2})\exp(-j\omega\ell_{BB,n_2}/c)/\ell_{BB,n_2}$$
$$-\sum_{n_3=1}^{N_{SS}}R_{SS,n_3}\sin(\theta_{SS,n_3})\cos(\theta_{SS,n_3})\exp(-jk\ell_{SS,n_3})\exp(-j\omega\ell_{SS,n_3}/c)/\ell_{SS,n_3}$$
$$-\sum_{n_4=1}^{N_{BS}}R_{BS,n_4}\sin(\theta_{BS,n_4})\cos(\theta_{BS,n_4})\exp(-jk\ell_{BS,n_4})\exp(-j\omega\ell_{BS,n_4}/c)/\ell_{BS,n_4}. \quad (14)$$

Regarding the powers of the transfer functions between a transmit dipole and a vector receiver, it is shown in Appendix II that $\Omega^d=\Omega_y^d+\Omega_z^d$. Here the powers are defined by $\Omega^d=E[|P^d(f)|^2]$, $\Omega_y^d=E[|P_y^d(f)|^2]$ and $\Omega_z^d=E[|P_z^d(f)|^2]$, where *d*=*z* or *y* indicates a transmit dipole in *z* or *y* direction, respectively. Using the derived channel transfer functions, various system parameters of interest can be calculated. For example, in the system of Section II.A with a dipole transmitter and a vector receiver, there are three channels listed in (8). Expressions are derived in Appendix II for powers and correlations of these channels, in terms of range, water depth, reflection coefficient, etc. Let $\rho_z^z=E[P^z(f)\{P_z^z(f)\}^*]$, $\rho_{zy}^z=E[P_z^z(f)\{P_y^z(f)\}^*]$ and $\rho_y^z=E[P^z(f)\{P_y^z(f)\}^*]$. Then we have the following equations derived in Appendix II

$$\Omega^z\approx\Omega_y^z\approx[(A_0^2+A^2)(1+|\beta|^6)+(16D_0^2-A_0^2-A^2)(|\beta|^2+|\beta|^4)]/[D_y^4(1-|\beta|^2)^3], \quad (15)$$

$$\begin{aligned}\Omega_z^z\approx&[(A_0^4+A^4)(1+|\beta|^{10})+(64D_0^4+48D_0^2(A_0^2+A^2)-3A_0^4-3A^4)(|\beta|^2+|\beta|^8)\\&+(704D_0^4-48D_0^2(A_0^2+A^2)+2A_0^4+2A^4)(|\beta|^4+|\beta|^6)]/[D_y^6(1-|\beta|^2)^5],\end{aligned} \quad (16)$$

$$\rho_z^z\approx\rho_{zy}^z\approx[(A^3-A_0^3)(1-|\beta|^8)+(2A_0^3-2A^3-24(A_0-A)D_0^2)(|\beta|^2-|\beta|^6)]/[D_y^5(1-|\beta|^2)^4], \quad (17)$$

$$\rho_y^z\approx[(A_0^2+A^2)(1+|\beta|^6)+(16D_0^2-A_0^2-A^2)(|\beta|^2+|\beta|^4)]/[D_y^4(1-|\beta|^2)^3], \quad (18)$$

where $|\beta|$ is not very small and $A=2D_0-z_0'-z_0$. The above results are numerically very close to the more complex expressions (57)-(62) derived in Appendix II.

Now we consider a numerical example, where the parameters are $D_0=81\,\text{m}$, $D_y=1000\,\text{m}$, $z_0'=25\,\text{m}$, $z_0=63\,\text{m}$, $L_{Tx}=L_{Rx}=0.2\lambda$ and $|\beta|=0.3162$, chosen according to [16] with the carrier frequency $f_0=12\,\text{kHz}$. The resulting correlation magnitudes of $\rho_z^z/\sqrt{\Omega^z\Omega_z^z}$, $\rho_{zy}^z/\sqrt{\Omega_z^z\Omega_y^z}$ and $\rho_y^z/\sqrt{\Omega^z\Omega_y^z}$ are 0.24, 0.24 and 1, respectively. The same correlation magnitudes are observed with $L_{Tx}=L_{Rx}=0.1\lambda$ and $L_{Tx}=L_{Rx}=0.5\lambda$. Plots of the normalized correlation magnitudes are provided in Fig. 3 versus z_0' and $|\beta|$. Fig. 3 shows that $\rho_z^z/\sqrt{\Omega^z\Omega_z^z}$ and $\rho_{zy}^z/\sqrt{\Omega_z^z\Omega_y^z}$ are insensitive to z_0' and decrease with $|\beta|$. On the other hand, $\rho_y^z/\sqrt{\Omega^z\Omega_y^z}$ is nearly independent of z_0' and $|\beta|$. The linear behavior of the two normalized

correlations ρ_z^z and ρ_{zy}^z for $|\beta|>0.4$ in Fig. 3(b) motivated us to obtain the following Taylor expansion around $|\beta|=1$

$$\rho_z^z / \sqrt{\Omega^z \Omega_z^z} \approx \rho_{zy}^z / \sqrt{\Omega_z^z \Omega_y^z} \approx (\sqrt{3}A^3 - 6\sqrt{3}A_0 D_0^2 + 6\sqrt{3}AD_0^2)(1-|\beta|)/(24 D_0^3). \quad (19)$$

According to Fig. 3(b), the linear approximation in (19) is very close to the nonlinear expressions in (14) and (17) for $|\beta|>0.4$.

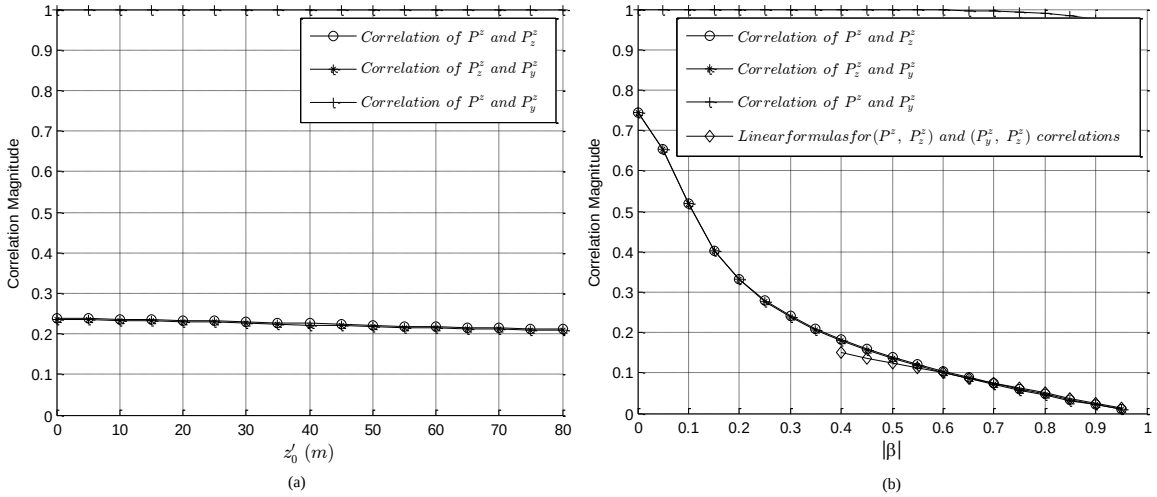

Fig. 3. Magnitudes of the normalized correlations between the three channels $P^z(f)$, $P_y^z(f)$ and $P_z^z(f)$ in Section III.A, (a) versus z_0', with $D_0=81\,\text{m}$, $D_y=1000\,\text{m}$, $z_0=63\,\text{m}$, $|\beta|=0.3126$, $f_0=12\text{kHz}$ and $L_{Tx}=L_{Rx}=0.2\lambda$, and (b) versus $|\beta|$, with $D_0=81\,\text{m}$, $D_y=1000\,\text{m}$, $z_0'=25\,\text{m}$, $z_0=63\,\text{m}$, $f_0=12\text{kHz}$ and $L_{Tx}=L_{Rx}=0.2\lambda$.

B. Statistical Multipath Channel Transfer Functions

In this subsection, we consider the case where the sea boundaries are relatively rough, scattering is the dominant mechanism and precise deterministic modeling is not feasible. A statistical channel model for a vector transducer receiver is developed in [11], where amplitudes, phases and angle of arrivals (AOAs) of rays are random variables. Here we extend the transfer functions of [11] to the scenarios where there is a transmit vector transducer, in addition to a receive vector transducer. Let the transmitter-receiver distance be large enough compared to the channel depth. Because of many times of scatterings of rays from surface and bottom over a long range from the transmitter to the receiver, one can consider the AOD and AOA of rays as independent random variables. Consider Fig. 4, where there is one scalar transmit transducer Tx_1 and one scalar receive transducer Rx_1. Denote the double-directional channel transfer function [23] [24] in frequency domain from Tx_1 to Rx_1 by $P_{11}(f)$. Similarly, consider another scalar transducer Tx_2 and another scalar transducer Rx_2, and let $P_{22}(f)$ denote the double-directional channel transfer function in frequency

domain from Tx_2 to Rx_2. The locations of Tx_2 and Rx_2 are (y_0', z_0') and (y_0, z_0), respectively. By definition, spatial correlation between $P_{11}(f)$ and $P_{22}(f)$ is $C_P(L_{Tx,z}, L_{Tx,y}, L_{Rx,z}, L_{Rx,y}) = E[P_{11}(f)P_{22}^*(f)]$. Similarly to Subsection III.A, in this double-directional channel there are four types of rays called *Bb*, *Ss*, *Bs* and *Sb*. The first letter is capital and indicates that the ray from the transmitter first hits the "B"ottom or "S"urface, whereas the second letter is small and specifies that the received ray's last scattering is from "b"ottom or "s"urface. Note that in [11] the focus is on the receive side, and therefore the received rays are divided into two groups. Since in this paper the transmitter is taken into account as well, the transmit rays are divided into two additional groups. Using the results of [11], the correlation in this double-directional channel can be written as (20), the product of transmit and receive correlations. Here $u_B(\theta^B)$ and $u_S(\theta^S)$ are the PDFs of the AODs in Fig. 4 impinging the sea bottom and surface, respectively, and $w_b(\gamma^b)$ and $w_s(\gamma^s)$ are the PDFs of the AOAs in Fig. 4 coming from the sea bottom and surface, respectively. AODs and AOAs are denoted by θ and γ, respectively, both measured with respect to the positive *y* axis, counterclockwise. The impact of a rough sea floor is included to some extent, by considering random bottom-scattered angle of departures and arrivals. The parameters $0 \le \Lambda_b \le 1$ and $1-\Lambda_b$ show what proportions of received rays are finally scattered from bottom and surface, respectively, whereas $0 \le \Lambda_B \le 1$ and $1-\Lambda_B$ indicate the proportions of transmitted rays that first hit the bottom and surface, respectively. We also have $L_{Tx,z} = L_{Tx}\sin(\theta_{Tx})$, $L_{Tx,y} = L_{Tx}\cos(\theta_{Tx})$, $L_{Rx,z} = L_{Rx}\sin(\gamma_{Rx})$ and $L_{Rx,y} = L_{Rx}\cos(\gamma_{Rx})$, with θ_{Tx} as the array direction at the transmit side and γ_{Rx} as the array direction at the receive side, respectively.

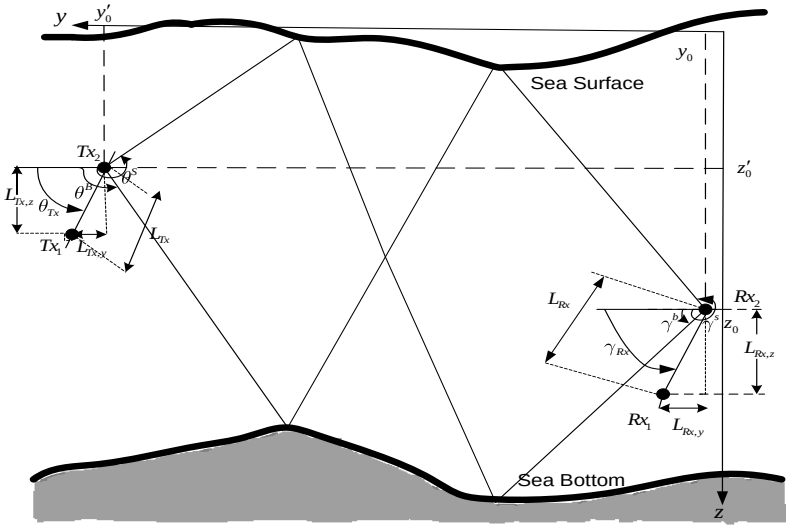

Fig. 4. Rays transmitted from two scalar transducers and received by two scalar transducers in a shallow water multipath channel.

Since particle velocity is the spatial gradient of the pressure, taking the derivatives of (20) with respect to $L_{Tx,z}$, $L_{Tx,y}$, $L_{Rx,z}$ and $L_{Rx,y}$, channel powers and possible correlations between the channels in the

proposed systems in (11) are derived in Appendix III. It is further shown in Appendix III that for the powers of the transfer functions between a transmit dipole and a vector receiver we $\Omega^d = \Omega_y^d + \Omega_z^d$. Here $d = z$ or y indicates a vertical or horizontal transmit dipole.

$$\begin{aligned} C_P(L_{Tx,z}, L_{Tx,y}, L_{Rx,z}, L_{Rx,y}) &= E[P_{11}(f)P_{22}^*(f)] = \{\Lambda_B \int_0^{\pi} u_B(\theta^B)\exp\{jk(L_{Tx,z}\sin(\theta^B) + L_{Tx,y}\cos(\theta^B))\}d\theta^B \\ &+(1-\Lambda_B)\int_{\pi}^{2\pi} u_S(\theta^S)\exp\{jk(L_{Tx,z}\sin(\theta^S) + L_{Tx,y}\cos(\theta^S))\}d\theta^S\} \\ &\times\{\Lambda_b \int_0^{\pi} w_b(\gamma^b)\exp\{jk(L_{Rx,z}\sin(\gamma^b) + L_{Rx,y}\cos(\gamma^b))\}d\gamma^b \\ &+(1-\Lambda_b)\int_{\pi}^{2\pi} w_s(\gamma^s)\exp\{jk(L_{Rx,z}\sin(\gamma^s) + L_{Rx,y}\cos(\gamma^s))\}d\gamma^s\}. \end{aligned} \tag{20}$$

Now we use the Gaussian angular model [11]. More specifically, there are two AOD random variables θ^B and θ^S, hitting the bottom and surface with parameters (μ_B, σ_B) and (μ_S, σ_S), respectively, where μ and σ denote the mean and standard deviation of a Gaussian distribution, respectively. Similarly, there are two AOA random variables γ^b and γ^s received from the bottom and surface, with parameters (μ_b, σ_b) and (μ_s, σ_s), respectively. As shown in Appendix III, the following relations can be obtained for the powers and possible correlations of the transfer functions between a transmit dipole and a receive dipole

$$\begin{aligned} \Omega_z^d &= \Omega^d\{\Lambda_b(\sin^2(\mu_b) + \sigma_b^2\cos^2(\mu_b)) + (1-\Lambda_b)(\sin^2(\mu_s) + \sigma_s^2\cos^2(\mu_s))\}, \\ \Omega_y^d &= \Omega^d\{\Lambda_b(\cos^2(\mu_b) + \sigma_b^2\sin^2(\mu_b)) + (1-\Lambda_b)(\cos^2(\mu_s) + \sigma_s^2\sin^2(\mu_s))\}. \end{aligned} \tag{21}$$

Here for $d = z$ and y, we have $\Omega^z = \Lambda_B(\sin^2(\mu_B) + \sigma_B^2\cos^2(\mu_B)) + (1-\Lambda_B)(\sin^2(\mu_S) + \sigma_S^2\cos^2(\mu_S))$ and $\Omega^y = \Lambda_B(\cos^2(\mu_B) + \sigma_B^2\sin^2(\mu_B)) + (1-\Lambda_B)(\cos^2(\mu_S) + \sigma_S^2\sin^2(\mu_S))$, respectively. Moreover

$$\begin{aligned} \rho_z^d &= \Omega^d\{\Lambda_b\sin(\mu_b) + (1-\Lambda_b)\sin(\mu_s)\}, \\ \rho_{zy}^d &= \Omega^d\{\Lambda_b(1-\sigma_b^2)\cos(\mu_b)\sin(\mu_b) + (1-\Lambda_b)(1-\sigma_s^2)\cos(\mu_s)\sin(\mu_s)\}, \\ \rho_y^d &= \Omega^d\{\Lambda_b\cos(\mu_b) + (1-\Lambda_b)\cos(\mu_s)\}. \end{aligned} \tag{22}$$

As a numerical example, magnitudes of normalized channel correlations $\rho_z^z / \sqrt{\Omega^z\Omega_z^z}$, $\rho_{zy}^z / \sqrt{\Omega_z^z\Omega_y^z}$ and $\rho_y^z / \sqrt{\Omega^z\Omega_y^z}$ for a transmit vertical dipole are , 0.28, 0.27 and 1, respectively. These are obtained for $L_{Tx} = L_{Rx} = 0.2\lambda$, $\mu_B = 17\pi/18\ (170^\circ)$, $\mu_S = 192\pi/180\ (192^\circ)$, $\mu_b = \pi/18\ (10^\circ)$, $\mu_s = 348\pi/180\ (348^\circ)$ and $\Lambda_B = \Lambda_b = 0.4$. For $L_{Tx} = L_{Rx} = 0.1\lambda$ and $L_{Tx} = L_{Rx} = 0.5\lambda$, similar correlation values are obtained. These correlations are relatively insensitive to small angle spreads, which we verified numerically.

IV. System Performance Analysis

Consider the proposed system with a vector transmitter and a vector receiver, whose input-output equations are derived in (11). Suppose the maximum number of taps in each channel is *M* and there are *K*

symbols to transmit from each transmitter. Then $\mathbf{p}^z = [p^z(0) \cdots p^z(M-1)\ 0 \cdots 0]^T$, $\mathbf{p}_y^z = [p_y^z(0) \cdots p_y^z(M-1)\ 0 \cdots 0]^T$ and $\mathbf{p}_z^z = [p_z^z(0) \cdots p_z^z(M-1)\ 0 \cdots 0]^T$ are the taps of the three channel impulse responses from the vertical transmit dipole to Rx_2 in (11), appended by $K-1$ zeros. Similarly, $\mathbf{p}^y = [p^y(0) \cdots p^y(M-1)\ 0 \cdots 0]^T$, $\mathbf{p}_y^y = [p_y^y(0) \cdots p_y^y(M-1)\ 0 \cdots 0]^T$ and $\mathbf{p}_z^y = [p_z^y(0) \cdots p_z^y(M-1)\ 0 \cdots 0]^T$ are the taps of the three channel impulse responses in (11) from the horizontal transmit dipole to Rx_2 appended by $K-1$ zeros. Also $\mathbf{p}_{12} = [p_{12}(0) \ldots p_{12}(M-1)\ 0 \cdots 0]^T$, $\mathbf{p}_y^{Tx_1} = [p_y^{Tx_1}(0) \ldots p_y^{Tx_1}(M-1)\ 0 \cdots 0]^T$ and $\mathbf{p}_z^{Tx_1} = [p_z^{Tx_1}(0) \ldots p_z^{Tx_1}(M-1)\ 0 \cdots 0]^T$ are the taps of the three channel impulse responses in (11) from Tx_1 to Rx_2. Then the channel matrices from a *z*-dipole, a *y*-dipole and a scalar pressure transmitter can be written as $\mathbf{H}^z = [\mathbf{H}_1^T\ \mathbf{H}_2^T\ \mathbf{H}_3^T]^\dagger$, $\mathbf{H}^y = j[\mathbf{H}_4^T\ \mathbf{H}_5^T\ \mathbf{H}_6^T]^\dagger$ and $\mathbf{H}^p = [\mathbf{H}_7^T\ \mathbf{H}_8^T\ \mathbf{H}_9^T]^\dagger$, respectively. Each matrix contains three submatrices because the receiver has a scalar pressure transducer, as well as a *y*-dipole and a *z*-dipole, as shown in Fig.1. Also each $\mathbf{H}_l$, $l = 1, 2, \cdots, 9$, is a circulant matrix of size $(K+M-1)\times(K+M-1)$ which has following structure

$$\mathbf{H}_l = \begin{pmatrix} h_l(0) & 0 & \cdots & 0 & h_l(M-1) & \cdots & h_l(1) \\ h_l(1) & h_l(0) & \cdots & 0 & 0 & \cdots & h_l(2) \\ \vdots & \vdots & \ddots & \vdots & \vdots & \ddots & \vdots \\ 0 & 0 & \cdots & h_l(M-1) & \vdots & \ddots & h_l(0) \end{pmatrix}, \ l = 1, 2, \cdots, 9, \tag{23}$$

where $h_1 = p^z$, $h_2 = p_y^z$ and $h_3 = p_z^z$, $h_4 = p^y$, $h_5 = p_y^y$, $h_6 = p_z^y$, $h_7 = p_{12}$, $h_8 = p_y^{Tx_1}$ and $h_9 = p_z^{Tx_1}$. Let the noise vector associated with Rx_2 and *y* and *z* receive dipole signals in (11) be $\mathbf{N} = [\mathbf{N}_2^T\ \mathbf{N}_y^T\ \mathbf{N}_z^T]^T$, where

$$\mathbf{N}_\ell = [\xi_\ell(0)\ \ \xi_\ell(1)\ \ \cdots\ \ \xi_\ell(K+M-2)]^T, \ \ell = 2,\ z,\ y. \tag{24}$$

Since the vector transmitter has a scalar transducer and two dipoles, we use a space-time block code (STBC) for three transmitters [25]. There are three *K*-symbol data streams, defined by $\mathbf{S}_i = [s_i(0)\ s_i(1)\ s_i(2) \cdots s_i(K-1)\ 0 \cdots 0]^T$, *i* = 1, 2, 3, each composed of *K* independent and identically distributed symbols and $M-1$ zeros. Upon applying a rate ¾ STBC [25] [26] to our vector transmitter, the received data over four time intervals can be written as

$$\begin{bmatrix} \bar{\bar{\mathbf{R}}}^{(1)} \\ \{\bar{\bar{\mathbf{R}}}^{(2)}\}^* \\ \{\bar{\bar{\mathbf{R}}}^{(3)}\}^* \\ \{\bar{\bar{\mathbf{R}}}^{(4)}\}^* \end{bmatrix} = \begin{bmatrix} \dot{\mathbf{H}}^p & \dot{\mathbf{H}}^z & \dot{\mathbf{H}}^y \\ \{\dot{\mathbf{H}}^z\}^* & -\{\dot{\mathbf{H}}^p\}^* & \mathbf{0} \\ \{\dot{\mathbf{H}}^y\}^* & \mathbf{0} & -\{\dot{\mathbf{H}}^p\}^* \\ \mathbf{0} & \{\dot{\mathbf{H}}^y\}^* & -\{\dot{\mathbf{H}}^z\}^* \end{bmatrix} \begin{bmatrix} \bar{\bar{\mathbf{S}}}_1 \\ \bar{\bar{\mathbf{S}}}_2 \\ \bar{\bar{\mathbf{S}}}_3 \end{bmatrix} + \begin{bmatrix} \bar{\bar{\mathbf{N}}}^{(1)} \\ \{\bar{\bar{\mathbf{N}}}^{(2)}\}^* \\ \{\bar{\bar{\mathbf{N}}}^{(3)}\}^* \\ \{\bar{\bar{\mathbf{N}}}^{(4)}\}^* \end{bmatrix}. \tag{25}$$

Here $\bar{\bar{\mathbf{S}}}_i = \mathbf{Q}\mathbf{S}_i$, *i* = 1, 2, 3, is the orthogonal discrete Fourier transform (DFT) of $\mathbf{S}_i$, with $\mathbf{Q}$ as the DFT matrix [26]. Additionally we have $\bar{\bar{\mathbf{R}}}^{(m)} = (\mathbf{I}_3 \otimes \mathbf{Q})\mathbf{R}^{(m)}$ and $\bar{\bar{\mathbf{N}}}^{(m)} = (\mathbf{I}_3 \otimes \mathbf{Q})\mathbf{N}^{(m)}$, *m* = 1, 2, 3, 4, where $\mathbf{I}_3$

is the 3×3 identity matrix. Note that $\mathbf{R}^{(m)}$ is the received signal vector during the *m*-th time interval, $m=1,\ 2,\ 3,\ 4$, defined by $\mathbf{R}^{(m)}=[r_2^{(m)}(0)\ \cdots\ r_2^{(m)}(K+M-2)\ r_y^{(m)}(0)\ \cdots\ r_y^{(m)}(K+M-2)\ r_z^{(m)}(0)\ \cdots\ r_z^{(m)}(K+M-2)]^T$, where $r_2^{(m)}$, $r_y^{(m)}$ and $r_z^{(m)}$ are the received pressure, *y*-velocity and *z*-velocity signals in (11) during the *m*-th time interval. Similarly, $\mathbf{N}^{(m)}=[\xi_2^{(m)}(0)\ \cdots\ \xi_2^{(m)}(K+M-2)\ \xi_y^{(m)}(0)\ \cdots\ \xi_y^{(m)}(K+M-2)\ \xi_z^{(m)}(0)\ \cdots\ \xi_z^{(m)}(K+M-2)]^T$, *m* = 1, 2, 3, 4, denotes the receiver noise vector over the *m*-th time interval. Additionally we have $\dot{\mathbf{H}}^z=[\dot{\mathbf{H}}_1^T\ \dot{\mathbf{H}}_2^T\ \dot{\mathbf{H}}_3^T]^\dagger$, $\dot{\mathbf{H}}^y=j[\dot{\mathbf{H}}_4^T\ \dot{\mathbf{H}}_5^T\ \dot{\mathbf{H}}_6^T]^\dagger$ and $\dot{\mathbf{H}}^p=[\dot{\mathbf{H}}_7^T\ \dot{\mathbf{H}}_8^T\ \dot{\mathbf{H}}_9^T]^T$, where $\dot{\mathbf{H}}_l=\mathbf{Q}\mathbf{H}_l\mathbf{Q}^*$, $l=1,2,\cdots,9$. Note that $\mathbf{H}_l$ is circulant and $\dot{\mathbf{H}}_l$ is diagonal. Finally, $\mathbf{0}$ is all-zero matrix.

Assuming perfect channel estimate at the receiver, here we use a zero forcing equalizer to investigate the feasibility of symbol detection in the proposed system in Fig. 1. Let us define

$$\boldsymbol{\mathcal{R}}=\begin{bmatrix}\dddot{\mathbf{R}}^{(1)}\\ \{\dddot{\mathbf{R}}^{(2)}\}^*\\ \{\dddot{\mathbf{R}}^{(3)}\}^*\\ \{\dddot{\mathbf{R}}^{(4)}\}^*\end{bmatrix},\quad \boldsymbol{\mathcal{H}}=\begin{bmatrix}\dot{\mathbf{H}}^p & \dot{\mathbf{H}}^z & \dot{\mathbf{H}}^y\\ \{\dot{\mathbf{H}}^z\}^* & -\{\dot{\mathbf{H}}^p\}^* & \mathbf{0}\\ \{\dot{\mathbf{H}}^y\}^* & \mathbf{0} & -\{\dot{\mathbf{H}}^p\}^*\\ \mathbf{0} & \{\dot{\mathbf{H}}^y\}^* & -\{\dot{\mathbf{H}}^z\}^*\end{bmatrix},$$

$$\boldsymbol{\mathcal{S}}=\begin{bmatrix}\dddot{\mathbf{S}}_1\\ \dddot{\mathbf{S}}_2\\ \dddot{\mathbf{S}}_3\end{bmatrix},\quad \boldsymbol{\mathcal{N}}=\begin{bmatrix}\dddot{\mathbf{N}}^{(1)}\\ \{\dddot{\mathbf{N}}^{(2)}\}^*\\ \{\dddot{\mathbf{N}}^{(3)}\}^*\\ \{\dddot{\mathbf{N}}^{(4)}\}^*\end{bmatrix}. \tag{26}$$

Then the received data vector in (25) can be written as $\boldsymbol{\mathcal{R}}=\boldsymbol{\mathcal{H}}\boldsymbol{\mathcal{S}}+\boldsymbol{\mathcal{N}}$. The minimum variance unbiased estimate of the transmitted symbol vector is [27]

$$\hat{\boldsymbol{\mathcal{S}}}=\ \boldsymbol{\mathcal{H}}^\dagger\boldsymbol{\mathcal{D}}^{-1}\boldsymbol{\mathcal{H}}^{\ -1}\boldsymbol{\mathcal{H}}^\dagger\boldsymbol{\mathcal{D}}^{-1}\boldsymbol{\mathcal{R}}, \tag{27}$$

where $\boldsymbol{\mathcal{D}}=E[\boldsymbol{\mathcal{N}}\boldsymbol{\mathcal{N}}^\dagger]$ is the covariance matrix of the noise vector $\boldsymbol{\mathcal{N}}$. The estimation error covariance matrix [27] for the vector $\boldsymbol{\mathcal{S}}$ can be written as

$$\boldsymbol{\mathcal{W}}=E[(\hat{\boldsymbol{\mathcal{S}}}-\boldsymbol{\mathcal{S}})(\hat{\boldsymbol{\mathcal{S}}}-\boldsymbol{\mathcal{S}})^\dagger]=\left(\boldsymbol{\mathcal{H}}^\dagger\boldsymbol{\mathcal{D}}^{-1}\boldsymbol{\mathcal{H}}\right)^{-1}. \tag{28}$$

Let $\boldsymbol{\Sigma}=E[\mathbf{N}^{(m)}\{\mathbf{N}^{(m)}\}^\dagger]$ be the covariance matrix of the $3(K+M-1)\times1$ noise vector $\mathbf{N}^{(m)}$, $m=1,2,3,4$. Then we have $\dddot{\boldsymbol{\Sigma}}=E[\dddot{\mathbf{N}}^{(m)}\{\dddot{\mathbf{N}}^{(m)}\}^\dagger]=(\mathbf{I}_3\otimes\mathbf{Q})\boldsymbol{\Sigma}(\mathbf{I}_3\otimes\mathbf{Q}^\dagger)$. Additionally, $\boldsymbol{\mathcal{D}}$ can be written as

$$\boldsymbol{\mathcal{D}}=\begin{bmatrix}\dddot{\boldsymbol{\Sigma}} & \mathbf{0} & \mathbf{0} & \mathbf{0}\\ \mathbf{0} & \dddot{\boldsymbol{\Sigma}}^* & \mathbf{0} & \mathbf{0}\\ \mathbf{0} & \mathbf{0} & \dddot{\boldsymbol{\Sigma}}^* & \mathbf{0}\\ \mathbf{0} & \mathbf{0} & \mathbf{0} & \dddot{\boldsymbol{\Sigma}}^*\end{bmatrix}, \tag{29}$$

which results in

$$\boldsymbol{\mathcal{W}} = \begin{bmatrix} \{\dot{\mathbf{H}}^p\}^\dagger \dot{\boldsymbol{\Sigma}}^{-1}\dot{\mathbf{H}}^p & \{\dot{\mathbf{H}}^p\}^\dagger \dot{\boldsymbol{\Sigma}}^{-1}\dot{\mathbf{H}}^z & \{\dot{\mathbf{H}}^p\}^\dagger \dot{\boldsymbol{\Sigma}}^{-1}\dot{\mathbf{H}}^y \\ +(\{\dot{\mathbf{H}}^y\}^\dagger \dot{\boldsymbol{\Sigma}}^{-1}\dot{\mathbf{H}}^y)^* & -(\{\dot{\mathbf{H}}^z\}^\dagger \dot{\boldsymbol{\Sigma}}^{-1}\dot{\mathbf{H}}^p)^* & -(\{\dot{\mathbf{H}}^y\}^\dagger \dot{\boldsymbol{\Sigma}}^{-1}\dot{\mathbf{H}}^p)^* \\ +(\{\dot{\mathbf{H}}^z\}^\dagger \dot{\boldsymbol{\Sigma}}^{-1}\dot{\mathbf{H}}^z)^* & & \\ \{\dot{\mathbf{H}}^z\}^\dagger \dot{\boldsymbol{\Sigma}}^{-1}\dot{\mathbf{H}}^p & (\{\dot{\mathbf{H}}^p\}^\dagger \dot{\boldsymbol{\Sigma}}^{-1}\dot{\mathbf{H}}^p)^* & \{\dot{\mathbf{H}}^z\}^\dagger \dot{\boldsymbol{\Sigma}}^{-1}\dot{\mathbf{H}}^y \\ -(\{\dot{\mathbf{H}}^p\}^\dagger \dot{\boldsymbol{\Sigma}}^{-1}\dot{\mathbf{H}}^z)^* & +(\{\dot{\mathbf{H}}^y\}^\dagger \dot{\boldsymbol{\Sigma}}^{-1}\dot{\mathbf{H}}^y)^* & -(\{\dot{\mathbf{H}}^y\}^\dagger \dot{\boldsymbol{\Sigma}}^{-1}\dot{\mathbf{H}}^z)^* \\ & +\{\dot{\mathbf{H}}^z\}^\dagger \dot{\boldsymbol{\Sigma}}^{-1}\dot{\mathbf{H}}^z & \\ \{\dot{\mathbf{H}}^y\}^\dagger \dot{\boldsymbol{\Sigma}}^{-1}\dot{\mathbf{H}}^p & \{\dot{\mathbf{H}}^y\}^\dagger \dot{\boldsymbol{\Sigma}}^{-1}\dot{\mathbf{H}}^z & (\{\dot{\mathbf{H}}^p\}^\dagger \dot{\boldsymbol{\Sigma}}^{-1}\dot{\mathbf{H}}^p)^* \\ -(\{\dot{\mathbf{H}}^p\}^\dagger \dot{\boldsymbol{\Sigma}}^{-1}\dot{\mathbf{H}}^y)^* & -(\{\dot{\mathbf{H}}^z\}^\dagger \dot{\boldsymbol{\Sigma}}^{-1}\dot{\mathbf{H}}^y)^* & +\{\dot{\mathbf{H}}^y\}^\dagger \dot{\boldsymbol{\Sigma}}^{-1}\dot{\mathbf{H}}^y \\ & & +(\{\dot{\mathbf{H}}^z\}^\dagger \dot{\boldsymbol{\Sigma}}^{-1}\dot{\mathbf{H}}^z)^* \end{bmatrix}^{-1}. \tag{30}$$

It is shown in Appendix IV that $\boldsymbol{\mathcal{W}}$ is a block diagonal matrix. Furthermore, the following closed-form expression is derived in Appendix IV for the estimation error covariance matrix of the data vector $\mathbf{S}_i$, $i = 1, 2, 3$

$$\begin{aligned} \mathbf{W} &= E[(\hat{\mathbf{S}}_i - \mathbf{S}_i)(\hat{\mathbf{S}}_i - \mathbf{S}_i)^\dagger] = (\{\mathbf{H}^p\}^\dagger \boldsymbol{\Sigma}^{-1}\mathbf{H}^p + \{\mathbf{H}^y\}^T \boldsymbol{\Sigma}^{-1}\{\mathbf{H}^y\}^* + \{\mathbf{H}^z\}^T \boldsymbol{\Sigma}^{-1}\{\mathbf{H}^z\}^*)^{-1} \\ &= \Delta(\mathbf{H}_1^\dagger\mathbf{H}_1 + 2\mathbf{H}_2^\dagger\mathbf{H}_2 + 2\mathbf{H}_3^\dagger\mathbf{H}_3 + \mathbf{H}_4^\dagger\mathbf{H}_4 + 2\mathbf{H}_5^\dagger\mathbf{H}_5 + 2\mathbf{H}_6^\dagger\mathbf{H}_6 + \mathbf{H}_7^\dagger\mathbf{H}_7 + 2\mathbf{H}_8^\dagger\mathbf{H}_8 + 2\mathbf{H}_9^\dagger\mathbf{H}_9)^{-1} \end{aligned}. \tag{31}$$

For binary phase shift keying (BPSK) modulation and similarly to [28] and [29], the average bit error rate (BER) for a block of size *K*, after the zero forcing equalization in (30) can be written as

$$\bar{P}_e = \frac{1}{K}\sum_{\kappa=1}^{K} Q(\sqrt{2\Omega_s / w_{\kappa\kappa}}). \tag{32}$$

Here $\Omega_s = E[|s_i(k)|^2] = 1$ is the average symbol power, *i* = 1, 2, 3, $w_{\kappa\kappa}$ is the κ-th diagonal element of $\mathbf{W}$ in (31) and $Q(x) = (2\pi)^{-1/2}\int_x^{+\infty}\exp(-x^2/2)dx$.

Channel Powers: Let $h(\tau)$ be a channel impulse response, with $H(f)$ as its Fourier transform. According to the properties of Bello functions [30] [31], the power of this channel is $\Omega = \int_{-\infty}^{\infty} E[|h(\tau)|^2]d\tau = E[|H(f)|^2]$. The powers of the channels in (11) are then given by $\Omega^d = E[|P^d(f)|^2]$, $\Omega_y^d = E[|P_y^d(f)|^2]$, $\Omega_z^d = E[|P_z^d(f)|^2]$, *d* = *y*, *z*, as well as $\Omega^p = E[|P_{12}(f)|^2]$, $\Omega_y^p = E[|P_y^{Tx_1}(f)|^2]$, and $\Omega_z^p = E[|P_z^{Tx_1}(f)|^2]$. As shown in Section III, we have $\Omega^d = \Omega_y^d + \Omega_z^d$, *d* = *y*, *z*. Also according to [10] and [11], $\Omega^p = \Omega_y^p + \Omega_z^p$.

Noise Powers: As shown in [10], for the isotropic noise model, the noise terms in (11) are uncorrelated, that is, $E[\xi_2\xi_y^*] = E[\xi_2\xi_z^*] = E[\xi_z\xi_y^*] = 0$. Moreover, for the powers of the noise terms in (11) we have $\Delta = E[|\xi_2|^2]$ and $\Delta_y = E[|\xi_y|^2] = \Delta_z = E[|\xi_z|^2] = \Delta/2$ [10].

Signal-to-Noise Ratios (SNRs): We notice that in the first time slot, $t = 1$, data is modulated on *p*, *y* and *z* channels by the transmit vector transducer and received by the *p* sensor of the receive vector transducer.

So, the average received SNR for the *p*-receiver and the first time slot is $\zeta(1)=(\Omega^p+\Omega^y+\Omega^z)/(3\Delta)$. For $t=1$, the average received SNRs for the *y* and *z* sensors of the vector receiver are, respectively, $\zeta_y(1)=(\Omega_y^p+\Omega_y^y+\Omega_y^z)/(3\Delta_y)$ and $\zeta_z(1)=(\Omega_z^p+\Omega_z^y+\Omega_z^z)/(3\Delta_z)$. In the second time slot and for the STBC used, data is modulated on *p* and *z* channels and received by *p*, *y* and *z* sensors. So, for $t=2$, average received SNRs by *p*, *y* and *z* sensors are $\zeta(2)=(\Omega^p+\Omega^z)/(2\Delta)$, $\zeta_y(2)=(\Omega_y^p+\Omega_y^z)/(2\Delta_y)$ and $\zeta_z(2)=(\Omega_z^p+\Omega_z^z)/(2\Delta_z)$, respectively. For $t=3$ and $t=4$ we similarly have $\zeta(3)=(\Omega^p+\Omega^y)/(2\Delta)$, $\zeta_y(3)=(\Omega_y^p+\Omega_y^y)/(2\Delta_y)$, $\zeta_z(3)=(\Omega_z^p+\Omega_z^y)/(2\Delta_z)$, and $\zeta(4)=(\Omega^y+\Omega^z)/(2\Delta)$, $\zeta_y(4)=(\Omega_y^y+\Omega_y^z)/(2\Delta_y)$, $\zeta_z(4)=(\Omega_z^y+\Omega_z^z)/(2\Delta_z)$. Since the vector receiver has three *p*, *y* and *z* sensors, the average SNR per receive channel over the *t*-th data block is $\bar{\zeta}(t)=(\zeta(t)+\zeta_y(t)+\zeta_z(t))/3,\ t=1,2,3,4$. Using the derived channel power relations $\Omega^p=\Omega_y^p+\Omega_z^p$, $\Omega^y=\Omega_y^y+\Omega_z^y$, $\Omega^z=\Omega_y^z+\Omega_z^z$, and the noise power relation $\Delta_y=\Delta_z=\Delta/2$, it can be shown that $\bar{\zeta}(1)=(\Omega^p+\Omega^y+\Omega^z)/(3\Delta)$, $\bar{\zeta}(2)=(\Omega^p+\Omega^z)/(2\Delta)$, $\bar{\zeta}(3)=(\Omega^p+\Omega^y)/(2\Delta)$, and $\bar{\zeta}(4)=(\Omega^y+\Omega^z)/(2\Delta)$. Let us define the average SNR per channel per data block by $\bar{\zeta}=(\bar{\zeta}(1)+\bar{\zeta}(2)+\bar{\zeta}(3)+\bar{\zeta}(4))/4$, which can be shown to be $\bar{\zeta}=(\Omega^p+\Omega^y+\Omega^z)/(3\Delta)$. With $\Omega^y+\Omega^z=\Omega^p$, $\bar{\zeta}$ for the proposed system with one vector transmitter and one vector receiver becomes $\bar{\zeta}=2\Omega^p/(3\Delta)$.

Using (32) and with $\Omega^p=3/2$, average BER $\bar{P}_e$ is plotted in Fig. 5 versus $\bar{\zeta}=1/\Delta$ for both channel types of Section III, with $K=200$ symbols, at a rate of 2400 bits/sec. As a reference, average BER of a system with three scalar transmitters and vector receiver is shown in Fig. 5 for both channels as well. The average SNR in this system is defined by first representing the powers of the channels stimulated by the three scalar transmitters Tx_1, Tx_2 and Tx_3 in Fig. 1 as $\Omega^p=E[|P_{12}(f)|^2]$, $\Omega^{Tx_2}=E[|P_{22}(f)|^2]$ and $\Omega^{Tx_3}=E[|P_{32}(f)|^2]$, respectively. Then upon replacing Ω^y and Ω^z in the above relations by Ω^{Tx_2} and Ω^{Tx_3}, respectively, and using these channel power relations for a scalar transmitter and a vector receiver $\Omega^p=\Omega_y^p+\Omega_z^p$, $\Omega^{Tx_2}=\Omega_y^{Tx_2}+\Omega_z^{Tx_2}$ and $\Omega^{Tx_3}=\Omega_y^{Tx_3}+\Omega_z^{Tx_3}$ [10], it can be similarly shown that $\bar{\zeta}=(\Omega^p+\Omega^{Tx_2}+\Omega^{Tx_3})/(3\Delta)$. With $\Omega^{Tx_2}=\Omega^{Tx_3}=\Omega^p/2$ and $\Omega^p=3/2$, the average SNR per channel per data block is $\bar{\zeta}=1/\Delta$, used to plot the average BER of the reference system in Fig. 5.

According to Fig. 5, BER of the proposed vector transmitter system is lower than the BER of the system with three scalar transmitters. When translated into SNR, the proposed system offers 2.5 dB and 0.5 dB gains in channel B and channel A, respectively.

System Degrees of Freedom: Degree of freedom [32] is a measure of diversity and spectral efficiency in multiple-input multiple-output (MIMO) systems. To understand the better performance of the proposed

vector transmit system, in Appendix V we have derived expressions for the degrees of freedom of the vector transmit system, χ_{vector}, and the system with three scalar transmitters, χ_{scalar}. As shown in Appendix V and summarized in (33), we have $\chi_{vector} > \chi_{scalar}$.

$$\begin{aligned}\chi_{vector} - \chi_{scalar} \approx (1-\Lambda_B)\sigma_S^2 + \Lambda_B\sigma_B^2 + 2(1-\Lambda_B)\Lambda_B(\pi-\mu_B)(\mu_S-\pi) \\ + (1-\Lambda_B)\Lambda_B[(\mu_B-\pi)^2 + (\mu_S-\pi)^2] > 0.\end{aligned} \tag{33}$$

The higher degrees of freedom in the vector transmit system justifies its better performance.

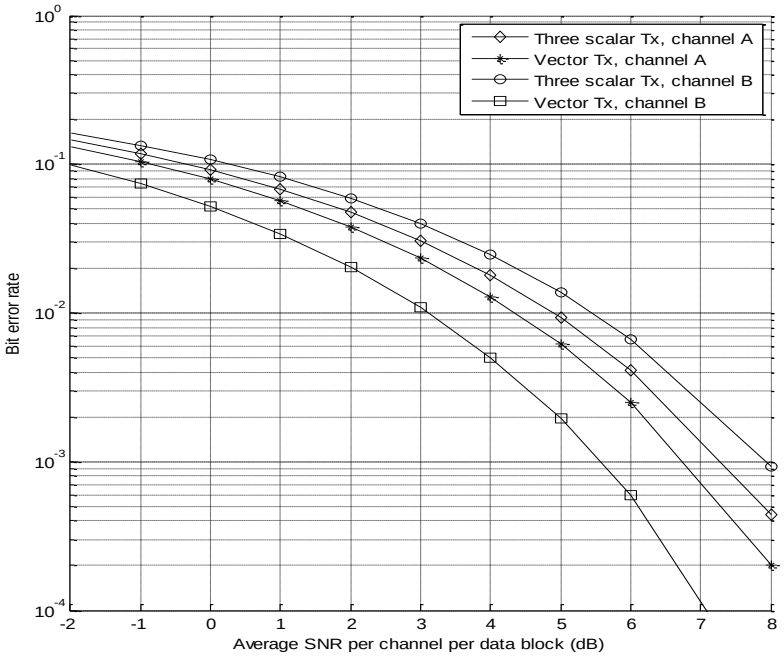

Fig. 5. Performance of the proposed system with a vector transmitter and a vector receiver, compared to a system with three scalar transmitters and a vector receiver, with $L_{Tx} = L_{Rx} = 0.225\lambda$. Parameters of channel A are $z_0' = 25\,\text{m}$, $z_0 = 63\,\text{m}$, $D_0 = 81\,\text{m}$, $D_y = 1000\,\text{m}$, $|\beta| = 0.7$ and $\alpha = 0.08$. Channel B parameters are $\sigma_B = \sigma_S = \sigma_b = \sigma_s = \pi/120\ (1.5^\circ)$, $\Lambda_B = \Lambda_b = 0.1$, $\mu_B = 11\pi/12\ (165^\circ)$, $\mu_S = 10\pi/9\ (200^\circ)$, $\mu_b = \pi/18\ (10^\circ)$ and $\mu_s = 348\pi/180\ (348^\circ)$.

V. Conclusion

In this paper, data transmission in particle velocity channels via acoustic vector transducers is proposed and investigated. First, system equations in the proposed communication system with a transmit vector transducer and a receive vector transducer are derived. Then two particle velocity channel transfer function models are developed to analyze the proposed system performance under different propagation conditions. Closed-form expressions are derived for possible channel correlations and system degrees of freedom. These parameters relate the channel characteristics to the system performance. Analytical studies and

simulation results show that a vector transducer transmitter can provide better performance than scalar transmitters. This can be attributed to the higher transmit diversity of the vector transmitter manifested in the higher degrees of freedom of the proposed system. The proposed system can be generalized to multiple transmit and receive vector transducers, frequency modulation methods [33], non-isotropic noise scenarios [33] and three-dimensional propagation where in addition to the *y* and *z* components of particle velocity, its *x* component can be utilized for signal transmission and reception as well.

APPENDIX I
CHARACTERIZATION OF CHANNELS IN THE PROPOSED SYSTEM FOR DIRECT PATHS

Consider Fig. 6, where there are three dipoles, one vertical at the transmit side and two at the receive side. The sizes of transmit and receive dipoles are $L_{Tx} \ll \lambda$ and $L_{Rx} \ll \lambda$, respectively. Let the size of each scalar transducer, a black circle, be much smaller than λ. Then the baseband acoustic pressure produced by a small spherical source of strength Γ_s at the point Tx_2 and measured at the point Rx_2 is given by [34]

$$p = (j\rho_0 ck\Gamma_s / (4\pi\ell_2))e^{-jk\ell_2}. \tag{34}$$

Here ℓ_2 is the distance between the points Tx_2 and Rx_2. Moreover, for ℓ_1 between Tx_1 and Rx_2 we have

$$\ell_1 = \sqrt{(\ell_2\cos\varphi - L_{Tx})^2 + (\ell_2\sin\varphi)^2} \approx \ell_2 - L_{Tx}\cos\varphi, \tag{35}$$

where the last expression is obtained because $L_{Tx} \ll \ell_2$. Also $0 < \varphi < 180^\circ$ is the departure angle at the transmit side of Fig. 6, measured with respect to the positive *z* axis, counterclockwise. Now let the two small spherical sources of equal strength and a 180 degree phase difference be placed at the points Tx_1 and Tx_2, i.e., Γ_s and $-\Gamma_s$, respectively, as shown in Fig. 6. Then the acoustic pressure produced by this dipole at the point Rx_2 and scaled by $(jkL_{Tx})^{-1}$ can be written as

$$\begin{aligned} p^z_{Rx_2} &= (jkL_{Tx})^{-1}((j\rho_0 ck\Gamma_s / (4\pi\ell_1))e^{-jk\ell_1} - (j\rho_0 ck\Gamma_s / (4\pi\ell_2))e^{-jk\ell_2}) \\ &= (jkL_{Tx})^{-1}(e^{jkL_{Tx}\cos\varphi} / [1 - (L_{Tx} / \ell_2)\cos\varphi] - 1) \times p \\ &\approx (jkL_{Tx})^{-1}(e^{jkL_{Tx}\cos\varphi} - 1) \times p \\ &= \cos\varphi \times p. \end{aligned} \tag{36}$$

The third line in (36) is obtained because $L_{Tx} \ll \ell_2$. The fourth line is obtained by simplifying the third line using the fact that $L_{Tx} \ll \lambda$, which gives $\cos(kL_{Tx}\cos\varphi) \approx 1$ and $\sin(kL_{Tx}\cos\varphi) \approx kL_{Tx}\cos\varphi$. On the other hand, using (35), (34) can be re-written as

$$p = (j\rho_0 ck\Gam_s / (4\pi\ell_2))e^{-jk(\ell_1 + L_{Tx}\cos\varphi)}. \tag{37}$$

By taking the derivative of p in (37) in the *z* direction we obtain

$$\begin{aligned} \partial p / \partial(-L_{Tx}) &= (-\rho_0 ck^2\Gamma_s / (4\pi\ell_2))e^{-jk\ell_2}\cos\varphi \\ &= jk\cos\varphi \times p. \end{aligned} \tag{38}$$

Comparison of the last lines of (36) and (38) shows

$$p^{z}_{Rx_2} = (jk)^{-1}\partial p / \partial(-L_{Tx}). \tag{39}$$

This result indicates that the pressure produced by a vertical transmit dipole upon $\Gamma_s / -\Gamma_s$ signaling is the same as the remote vertical spatial gradient of the pressure that would have been produced by a single transmitter of strength Γ_s located at the point Tx_2 in Fig. 6.

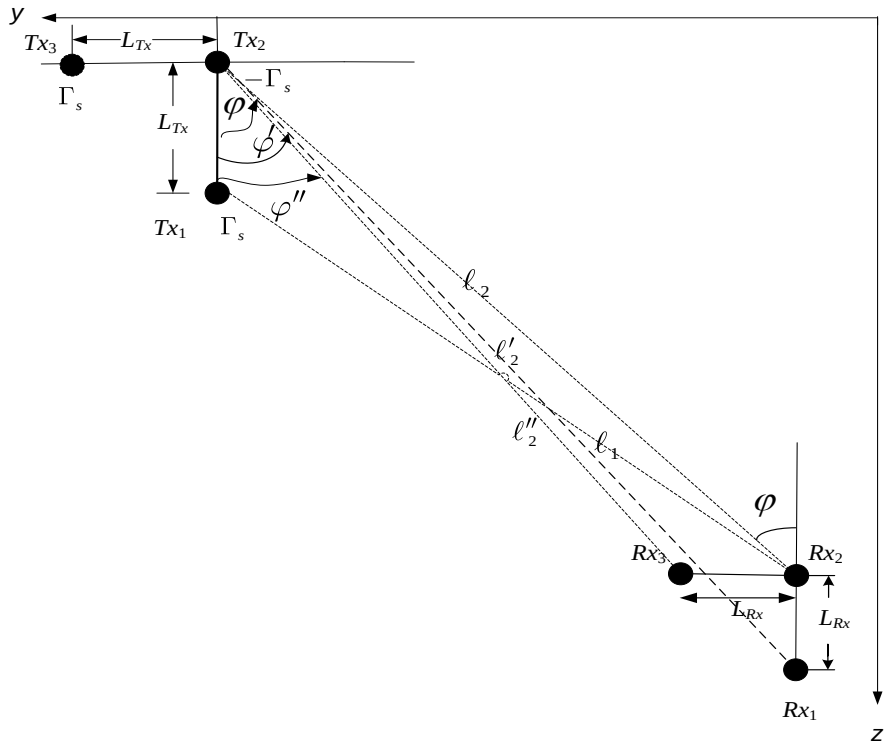

Fig.6. Direct paths in the system with two transmit dipoles and two receive dipoles.

Now we investigate the signals produced by the transmit vertical dipole and measured by the receive vertical dipole. An expression for the signal measured by the receive horizontal dipole is given in (46). The distance between the points Tx_2 and Rx_1 in Fig. 6 can be written as

$$\ell'_2 = \sqrt{(\ell_2 \cos\varphi + L_{Rx})^2 + (\ell_2 \sin\varphi)^2} \approx \ell_2 + L_{Rx}\cos\varphi. \tag{40}$$

Also similarly to (36), the acoustic pressure produced by the vertical dipole at the point Rx_1 and scaled by $(jkL_{Tx})^{-1}$ can be written as

$$p^{z}_{Rx_1} = (j\rho_0 ck\Gamma_s / (4\pi\ell'_2))e^{-jk\ell'_2}\cos\varphi'. \tag{41}$$

By subtracting (36) from (41) and since $\varphi' \approx \varphi$, the spatial gradient measured by the receive vertical dipole and scaled by $(jkL_{Rx})^{-1}$ can be written as

$$\begin{aligned}(jkL_{Rx})^{-1}(p^{z}_{Rx_1} - p^{z}_{Rx_2}) &\approx (jkL_{Rx})^{-1}(j\rho_0 ck\Gamma_s / (4\pi))\cos\varphi \times (e^{-jk\ell'_2} / \ell'_2 - e^{-jk\ell_2} / \ell_2) \\ &\approx (jkL_{Rx})^{-1}(j\rho_0 ck\Gamma_s / (4\pi\ell_2))e^{-jk\ell_2}\cos\varphi \times (e^{-jkL_{Rx}\cos\varphi} - 1) \\ &= -(j\rho_0 ck\Gamma_s / (4\pi\ell_2))e^{-jk\ell_2}\cos^2\varphi \\ &= -\cos^2\varphi \times p.\end{aligned} \tag{42}$$

The second line in (42) is obtained by replacing ℓ_2' using (40) and noticing that $L_{Rx} \ll \ell_2$. Since $L_{Rx} \ll \lambda$, we have $\cos kL_{Rx}\cos\varphi \approx 1$ and $\sin kL_{Rx}\cos\varphi \approx kL_{Rx}\cos\varphi$. Thus, the second line in (42) simplifies to the third line there. Using (34), the fourth line in (42) can be finally obtained.

On the other hand, upon using (40), p in (34) can be written as

$$p = (j\rho_0 ck\Gamma_s / (4\pi\ell_2))e^{-jk(\ell_2' - L_{Rx}\cos\varphi)}. \tag{43}$$

According to the definition of particle acceleration [35], second vertical spatial derivative of p in (43) gives the particle acceleration at the point Rx_2, produced by the pressure transmitter at the point Tx_2

$$\partial^2 p / \partial(-L_{Rx})^2 = (jk)^2 \cos^2\varphi \times p. \tag{44}$$

Comparison of the last line of (42) and (44) results in

$$(jkL_{Rx})^{-1}(p^z_{Rx_1} - p^z_{Rx_2}) = -(jk)^{-2}\partial^2 p / \partial(-L_{Rx})^2. \tag{45}$$

This means the particle velocity produced by a dipole upon $\Gamma_s / -\Gamma_s$ signaling and measured by a dipole at the receiver is equivalent to the particle acceleration that would have been generated by a single transmitter of strength Γ_s located at the point Tx_2 in Fig. 6.

Equations (36) and (42) correspond to a scalar receiver and a vertical dipole receiver, respectively, while the transmitter is a vertical dipole. These and equations for other configurations, i.e., vertical transmit/horizontal receive dipoles, horizontal transmit dipole/scalar receiver, horizontal transmit/vertical receive dipoles and horizontal transmit/horizontal receive dipoles are summarized in Table II. The last four entries are derived in [36] similarly to (36) and (42).

TABLE II
DIRECT PATH CHANNELS FOR VARIOUS TRANSMIT AND RECEIVE CONFIGURATIONS

Channel Definition	Channel Equation
Acoustic pressure produced by the vertical dipole at the point Rx_2	$p^z_{Rx_2} = \cos\varphi \times p$ (36)
Acoustic pressure gradient produced by the vertical dipole and measured by the vertical receive dipole	$(jkL_{Rx})^{-1}(p^z_{Rx_1} - p^z_{Rx_2}) = -\cos^2\varphi \times p$ (42)
Acoustic pressure gradient produced by the vertical dipole and measured by the horizontal receive dipole	$(jkL_{Rx})^{-1}(p^z_{Rx_3} - p^z_{Rx_2}) = \cos\varphi\sin\varphi \times p$ (46)
Acoustic pressure produced by the horizontal dipole at the point Rx_2	$p^y_{Rx_2} = \cos\theta \times p$ (47)
Acoustic pressure gradient produced by the horizontal dipole and measured by the vertical receive dipole	$(jkL_{Rx})^{-1}(p^y_{Rx_1} - p^y_{Rx_2}) = -\cos\theta\sin\theta \times p$ (48)
Acoustic pressure gradient produced by the horizontal dipole and measured by the horizontal receive dipole	$(jkL_{Rx})^{-1}(p^y_{Rx_3} - p^y_{Rx_2}) = -\cos^2\theta \times p$ (49)

For the last three entries in Table II where the transmit dipole is horizontal, i.e., the pair $\{Tx_2, Tx_3\}$ in Fig. 6, the departure angle $90^\circ < \theta < 270^\circ$ is measured with respect to the positive *y* axis, counterclockwise.

APPENDIX II
GEOMETRICAL MULTIPATH CHANNEL TRANSFER FUNCTIONS AND THEIR PROPERTIES

For the channel model in Subsection III.A, as shown in Fig. 2, $A_{XW,n}$ is given by (50) for the *n*-th ray from the *XW* group, where $X, W = S$ or B. The combined pressure loss is given by (51) and for each path from Tx_2 to Rx_2, the angle of departure (AOD) $\theta_{XW,n}$ is given in (52).

$$\begin{aligned} A_{SB,n} &= 2nD_0 + z_0' - z_0, \qquad A_{BB,n} = 2nD_0 - z_0' - z_0, \\ A_{SS,n} &= 2(n-1)D_0 + z_0' + z_0, A_{BS,n} = 2nD_0 - z_0' + z_0. \end{aligned} \tag{50}$$

$$R_{SB,n} \approx |\beta|^n, \quad R_{BB,n} \approx -|\beta|^{n-1}, \quad R_{SS,n} \approx -|\beta|^n, \quad R_{BS,n} \approx |\beta|^n. \tag{51}$$

$$\begin{aligned} \theta_{SB,n} &= \pi + \arctan(A_{SB,n} / D_y), \ \theta_{BB,n} = \pi - \arctan(A_{BB,n} / D_y), \\ \theta_{SS,n} &= \pi + \arctan(A_{SS,n} / D_y), \ \theta_{BS,n} = \pi - \arctan(A_{BS,n} / D_y). \end{aligned} \tag{52}$$

Now let the transmitter be a vertical dipole, where the depths of the two transducers of the dipole, Tx_1 and Tx_2 in Fig. 2, are $z_0' + L_{Tx}$ and z_0', respectively. Here $L_{Tx} \ll \lambda$ and $L_{Tx} \ll \ell_{XW,n}$, for all *n*, *X* and *W*, where $\ell_{XW,n}$ is defined in Section III.A as the *n*-th path length of the *XW* ray from Tx_2 to Rx_2. The image of the transmit dipole, with the images of Tx_1 and Tx_2 labeled as $\hat{T}x_1$ and $\hat{T}x_2$ are shown in Fig. 2 for different types of rays. The acoustic pressure produced by the vertical transmit dipole at the point Rx_2 through a path of length ℓ and scaled by $(jkL_{Tx})^{-1}$ can be calculated by substituting (34) into (36). This gives

$$p^z(\tau) = \cos\varphi \exp(-jk\ell)\ell^{-1}\delta(\tau - \ell / c), \tag{53}$$

where the constant term $j\rho_0 ck\Gamma_s / (4\pi)$ is not considered, to simplify the notation without loss of generality, and ℓ / c is the travel time. This resembles the baseband impulse response of a single path wireless channel [37]. By taking the Fourier transform with respect to τ, the single-path baseband transfer function of the dipole pressure-equivalent channel in frequency domain can be written as $P^z(f) = \cos\varphi \exp(-jk\ell)\ \ell^{-1}\exp(-j\omega\ell / c)$, where $\omega = 2\pi f$.

For the vertical transmit dipole and with $\varphi_0 = \theta_0 - 90^\circ$, the direct path pressure-equivalent dipole transfer function in frequency domain becomes $\sin(\theta_0)\exp(-jk\ell_0)\exp(-j\omega\ell_0 / c)\ell_0^{-1}$. For an *XW* ray, $X, W = S$ or B, the baseband pressure-equivalent channel transfer function originated from the dipole image $(\hat{T}x_1, \hat{T}x_2)$ towards Rx_2 can be similarly written as $R_{XW,n}\cos(\varphi_{XW,n}) \times \exp(-jk\ell_{XW,n})\ell_{XW,n}^{-1}\exp(-j\omega\ell_{XW,n} / c)$, where $R_{XW,n}$ incorporates the loss due to multiple interactions with surface and bottom, as listed in (51). For *BB* and *SS* rays, this expression should be multiplied by a negative sign. This is because in Fig. 6 the strength of the sources Tx_2 and Tx_1, with Tx_2 above Tx_1, are $-\Gamma_s$

and Γ_s, respectively. However, since for *SS* and *BB* rays in Fig. 2 (c) and 2 (b), respectively, $\hat{T}x_2$ with strength $-\Gamma_s$ is below $\hat{T}x_1$, the first line in (36) and the fourth line in (36) should be multiplied by a negative sign. To proceed further, each $\varphi_{XW,n}$ needs to be replaced by the AOD $\theta_{XW,n}$, according to these relations obtained from Fig. 2: $\varphi_{SB,n} = \theta_{SB,n} - 90^\circ$, $\varphi_{BB,n} = 270^\circ - \theta_{BB,n}$, $\varphi_{SS,n} = 270^\circ - \theta_{SS,n}$ and $\varphi_{BS,n} = \theta_{BS,n} - 90^\circ$. Superposition of these components produced by the vertical dipole and its images results in the baseband pressure-equivalent channel transfer function (12) at Rx_2. Note that $\ell_{XW,n}$, $R_{XW,n}$ and $\theta_{XW,n}$ can be obtained from (50)-(52), respectively. Also N_{SB}, N_{BB}, N_{SS} and N_{BS} denote the number of rays in each group such that $N_{SB} = \max\{n_1 \,||\, R_{SB,n_1}\ell_0 / \ell_{SB,n_1} | \geq \alpha\}$, $N_{BB} = \max\{n_2 \,||\, R_{BB,n_2}\ell_0 / \ell_{BB,n_2} \geq \alpha|\}$, $N_{SS} = \max\{n_3 \,||\, R_{SS,n_3}\ell_0 / \ell_{SS,n_3} | \geq \alpha\}$ and $N_{BS} = \max\{n_4 \,||\, R_{BS,n_4}\ell_0 / \ell_{BS,n_4} | \geq \alpha\}$, where $0 < \alpha \leq 1$ is a parameter such that rays with amplitudes less than $100\alpha\%$ of the amplitude of the direct path, $1/\ell_0$, will not be considered in numerical simulations. Typically $\alpha \ll 1$. For $\alpha = 0$ usually all *N*'s become large.

Now consider the receive vertical dipole in Fig. 2, where the depth of the two transducers of the dipole, Rx_1 and Rx_2, are $z_0 + L_{Rx}$ and z_0, respectively. The spatial gradient measured by this receive dipole which is at a distance ℓ from the transmit dipole can be determined by substituting (34) into the fourth line in (42). This gives $(jkL_{Rx})^{-1}(p^z_{Rx_1}(\tau) - p^z_{Rx_2}(\tau)) = -\cos^2\varphi \exp(-jk\ell)\ell^{-1}\delta(\tau - \ell/c)$, where the constant term $j\rho_0 ck\Gamma_s/(4\pi)$ is not considered, to simplify the notation. This is the baseband impulse response of a single path channel initiated by a vertical transmit dipole and seen by a vertical receive dipole. Fourier transform of this with respect to τ results in the single-path pressure-equivalent baseband channel transfer function in frequency domain as $P^z_z(f) = (jkL_{Rx})^{-1}(P^z_{Rx_1}(f) - P^z_{Rx_2}(f)) = -\cos^2\varphi \times \exp(-jk\ell)\ell^{-1}\exp(-j\omega\ell/c)$. Also for *BB* and *SS* rays, this expression should be multiplied by a negative sign. Then we need to write φ in terms of θ for different types of rays, as discussed previously, and also replace ℓ with ℓ_0 and $\ell_{XW,n}$. Superposition of the resulting components provides (13) for the baseband pressure-equivalent channel transfer function between the vertical transmit dipole and the vertical receive dipole.

The horizontal receive dipole in Fig. 2 includes the transducer Rx_3 at $(y_0 + L_{Rx}, z_0)$. By substituting (34) into (46), an expression for the single-path baseband pressure-equivalent channel transfer function between the transmit vertical dipole and receive horizontal dipole, i.e., $P^z_y(f) = (jkL_{Rx})^{-1}(P^z_{Rx_3}(f) - P^z_{Rx_2}(f))$ can be obtained. Similarly to (13), superposition of such expressions ultimately results in (14).

Now we consider a horizontal transmit dipole. Following the same approach that results in (12)-(14), equations (47), (48) and (49) can be similarly used to obtain the following expressions. Equations (54)-(56)

are the baseband pressure-equivalent channel transfer functions between a horizontal transmit dipole and a scalar transducer and two dipoles at the receive side.

$$P^y(f)=\cos(\theta_0)\exp(-jk\ell_0)\exp(-j\omega\ell_0/c)/\ell_0 \ +\sum_{n_1=1}^{N_{SB}}R_{SB,n_1}\cos(\theta_{SB,n_1})\exp(-jk\ell_{SB,n_1})\exp(-j\omega\ell_{SB,n_1}/c)/\ell_{SB,n_1}$$
$$+\sum_{n_2=1}^{N_{BB}}R_{BB,n_2}\cos(\theta_{BB,n_2})\exp(-jk\ell_{BB,n_2})\exp(-j\omega\ell_{BB,n_2}/c)/\ell_{BB,n_2}$$
$$+\sum_{n_3=1}^{N_{SS}}R_{SS,n_3}\cos(\theta_{SS,n_3})\exp(-jk\ell_{SS,n_3})\exp(-j\omega\ell_{SS,n_3}/c)/\ell_{SS,n_3}$$
$$+\sum_{n_4=1}^{N_{BS}}R_{BS,n_4}\cos(\theta_{BS,n_4})\exp(-jk\ell_{BS,n_4})\exp(-j\omega\ell_{BS,n_4}/c)/\ell_{BS,n_4}. \quad (54)$$

$$P_z^y(f)=-\cos(\theta_0)\sin(\theta_0)\exp(-jk\ell_0)\exp(-j\omega\ell_0/c)/\ell_0 \ -\sum_{n_1=1}^{N_{SB}}R_{SB,n_1}\cos(\theta_{SB,n_1})\sin(\theta_{SB,n_1})\exp(-jk\ell_{SB,n_1})\exp(-j\omega\ell_{SB,n_1}/c)/\ell_{SB,n_1}$$
$$-\sum_{n_2=1}^{N_{BB}}R_{BB,n_2}\cos(\theta_{BB,n_2})\sin(\theta_{BB,n_2})\exp(-jk\ell_{BB,n_2})\exp(-j\omega\ell_{BB,n_2}/c)/\ell_{BB,n_2}$$
$$-\sum_{n_3=1}^{N_{SS}}R_{SS,n_3}\cos(\theta_{SS,n_3})\sin(\theta_{SS,n_3})\exp(-jk\ell_{SS,n_3})\exp(-j\omega\ell_{SS,n_3}/c)/\ell_{SS,n_3}$$
$$-\sum_{n_4=1}^{N_{BS}}R_{BS,n_4}\cos(\theta_{BS,n_4})\sin(\theta_{BS,n_4})\exp(-jk\ell_{BS,n_4})\exp(-j\omega\ell_{BS,n_4}/c)/\ell_{BS,n_4}. \quad (55)$$

$$P_y^y(f)=-\cos^2(\theta_0)\exp(-jk\ell_0)\exp(-j\omega\ell_0/c)/\ell_0 \ -\sum_{n_1=1}^{N_{SB}}R_{SB,n_1}\cos^2(\theta_{SB,n_1})\exp(-jk\ell_{SB,n_1})\exp(-j\omega\ell_{SB,n_1}/c)/\ell_{SB,n_1}$$
$$-\sum_{n_2=1}^{N_{BB}}R_{BB,n_2}\cos^2(\theta_{BB,n_2})\exp(-jk\ell_{BB,n_2})\exp(-j\omega\ell_{BB,n_2}/c)/\ell_{BB,n_2}$$
$$-\sum_{n_3=1}^{N_{SS}}R_{SS,n_3}\cos^2(\theta_{SS,n_3})\exp(-jk\ell_{SS,n_3})\exp(-j\omega\ell_{SS,n_3}/c)/\ell_{SS,n_3}$$
$$-\sum_{n_4=1}^{N_{BS}}R_{BS,n_4}\cos^2(\theta_{BS,n_4})\exp(-jk\ell_{BS,n_4})\exp(-j\omega\ell_{BS,n_4}/c)/\ell_{BS,n_4}. \quad (56)$$

A. Channel Powers

The path phases of the channels $P^z(f)$, $P_z^z(f)$ and $P_y^z(f)$ in (12)-(14), respectively, are given by $k\ell_0=2\pi\ell_0/\lambda$ and $k\ell_{XW,n}=2\pi\ell_{XW,n}/\lambda$. These path phases change by 2π, when their path lengths vary by a wavelength. Since there are large variations in these path lengths, path phases change over a wide range. When reduced to module 2π, they can be accurately modeled by uniform probability density functions (PDFs) over $[0,2\pi)$ [38] [39]. Then, following the same method developed in [11], average powers of $P^z(f)$, $P_z^z(f)$ and $P_y^z(f)$ can be written as

$$\Omega^z = E[|P^z(f)|^2] = \sin^2(\theta_0)\cos^2(\theta_0)/D_y^2$$
$$+\sum_{n_1=1}^{N_{SB}} |\beta|^{2n_1} \sin^2(\theta_{SB,n_1})\cos^2(\theta_{SB,n_1})/D_y^2 + \sum_{n_2=1}^{N_{BB}} |\beta|^{2(n_2-1)} \sin^2(\theta_{BB,n_2})\cos^2(\theta_{BB,n_2})/D_y^2 \quad (57)$$
$$+\sum_{n_3=1}^{N_{SS}} |\beta|^{2n_3} \sin^2(\theta_{SS,n_3})\cos^2(\theta_{SS,n_3})/D_y^2 + \sum_{n_4=1}^{N_{BS}} |\beta|^{2n_4} \sin^2(\theta_{BS,n_4})\cos^2(\theta_{BS,n_4})/D_y^2,$$

$$\Omega_z^z = E[|P_z^z(f)|^2] = \sin^4(\theta_0)\cos^2(\theta_0)/D_y^2$$
$$+\sum_{n_1=1}^{N_{SB}} |\beta|^{2n_1} \sin^4(\theta_{SB,n_1})\cos^2(\theta_{SB,n_1})/D_y^2 + \sum_{n_2=1}^{N_{BB}} |\beta|^{2(n_2-1)} \sin^4(\theta_{BB,n_2})\cos^2(\theta_{BB,n_2})/D_y^2 \quad (58)$$
$$+\sum_{n_3=1}^{N_{SS}} |\beta|^{2n_3} \sin^4(\theta_{SS,n_3})\cos^2(\theta_{SS,n_3})/D_y^2 + \sum_{n_4=1}^{N_{BS}} |\beta|^{2n_4} \sin^4(\theta_{BS,n_4})\cos^2(\theta_{BS,n_4})/D_y^2,$$

$$\Omega_y^z = E[|P_y^z(f)|^2] = \sin^2(\theta_0)\cos^4(\theta_0)/D_y^2$$
$$+\sum_{n_1=1}^{N_{SB}} |\beta|^{2n_1} \sin^2(\theta_{SB,n_1})\cos^4(\theta_{SB,n_1})/D_y^2 + \sum_{n_2=1}^{N_{BB}} |\beta|^{2(n_2-1)} \sin^2(\theta_{BB,n_2})\cos^4(\theta_{BB,n_2})/D_y^2 \quad (59)$$
$$+\sum_{n_3=1}^{N_{SS}} |\beta|^{2n_3} \sin^2(\theta_{SS,n_3})\cos^4(\theta_{SS,n_3})/D_y^2 + \sum_{n_4=1}^{N_{BS}} |\beta|^{2n_4} \sin^2(\theta_{BS,n_4})\cos^4(\theta_{BS,n_4})/D_y^2,$$

where $R_{XW,n}$ in (12)-(14) is written in terms of β using (51). Moreover, using the definitions of ℓ_0, $\ell_{XW,n}$, θ_0, $\theta_{XW,n}$ and the relations in (50), path lengths are expressed in terms of AODs, i.e., $\ell_0 = -D_y/\cos(\theta_0)$ and $\ell_{XW,n} = -D_y/\cos(\theta_{XW,n})$, $\theta_0,\ \theta_{XW,n} \in (\pi/2, 3\pi/2)$. Inspection of (57)-(59) reveals that $\Omega^z = \Omega_y^z + \Omega_z^z$ for the vertical transmit dipole. For the horizontal transmit dipole and using (54)-(56) it can be similarly shown that $\Omega^y = \Omega_y^y + \Omega_z^y$.

B. Channel Correlations

Similarly to the previous subsection, average correlations between $P^z(f)$, $P_z^z(f)$ and $P_y^z(f)$ in (12)-(14) can be written as

$$\rho_z^z = E[P^z(f)\{P_z^z(f)\}^*] = -\sin^3(\theta_0)\cos^2(\theta_0)/D_y^2$$
$$-\sum_{n_1=1}^{N_{SB}} |\beta|^{2n_1} \sin^3(\theta_{SB,n_1})\cos^2(\theta_{SB,n_1})/D_y^2 + \sum_{n_2=1}^{N_{BB}} |\beta|^{2(n_2-1)} \sin^3(\theta_{BB,n_2})\cos^2(\theta_{BB,n_2})/D_y^2 \quad (60)$$
$$+\sum_{n_3=1}^{N_{SS}} |\beta|^{2n_3} \sin^3(\theta_{SS,n_3})\cos^2(\theta_{SS,n_3})/D_y^2 - \sum_{n_4=1}^{N_{BS}} |\beta|^{2n_4} \sin^3(\theta_{BS,n_4})\cos^2(\theta_{BS,n_4})/D_y^2,$$

$$\rho_{zy}^z = E[P_z^z(f)\{P_y^z(f)\}^*] = \sin^3(\theta_0)\cos^3(\theta_0)/D_y^2$$
$$+\sum_{n_1=1}^{N_{SB}} |\beta|^{2n_1} \sin^3(\theta_{SB,n_1})\cos^3(\theta_{SB,n_1})/D_y^2 - \sum_{n_2=1}^{N_{BB}} |\beta|^{2(n_2-1)} \sin^3(\theta_{BB,n_2})\cos^3(\theta_{BB,n_2})/D_y^2 \quad (61)$$
$$-\sum_{n_3=1}^{N_{SS}} |\beta|^{2n_3} \sin^3(\theta_{SS,n_3})\cos^3(\theta_{SS,n_3})/D_y^2 + \sum_{n_4=1}^{N_{BS}} |\beta|^{2n_4} \sin^3(\theta_{BS,n_4})\cos^3(\theta_{BS,n_4})/D_y^2,$$

$$\rho_y^z = E[P^z(f)\{P_y^z(f)\}^*] = -\sin^2(\theta_0)\cos^3(\theta_0)/D_y^2$$
$$-\sum_{n_1=1}^{N_{SB}} |\beta|^{2n_1} \sin^2(\theta_{SB,n_1})\cos^3(\theta_{SB,n_1})/D_y^2 - \sum_{n_2=1}^{N_{BB}} |\beta|^{2(n_2-1)} \sin^2(\theta_{BB,n_2})\cos^3(\theta_{BB,n_2})/D_y^2 \quad (62)$$
$$-\sum_{n_3=1}^{N_{SS}} |\beta|^{2n_3} \sin^2(\theta_{SS,n_3})\cos^3(\theta_{SS,n_3})/D_y^2 - \sum_{n_4=1}^{N_{BS}} |\beta|^{2n_4} \sin^2(\theta_{BS,n_4})\cos^3(\theta_{BS,n_4})/D_y^2.$$

To obtain further insight, now we consider the case when $|\beta|$ is not very small. This way all the N's in (57)-(62) can be considered to be large. With $D_y / D_0 \gg 2n+1$, $n = 1, 2, \cdots$, $\cos(\theta) \approx 1$ and $\sin(\theta) \approx \theta$ for small θ, summations in (57)-(62) can be simplified to equations (15)-(18).

APPENDIX III
STATISTICAL MULTIPATH CHANNEL TRANSFER FUNCTIONS AND THEIR PROPERTIES

Regarding the channel model in Subsection III.B, first we derive some general expressions for a dipole transmitter and a vector receiver. Based on the channel definitions after (8) and (11) and as $L_{Tx} \to 0$ we have $P^d(f) = (jk)^{-1}\partial P(f)/\partial L_{Tx,d}$. Here $P(f)$ is the acoustic pressure measured by a scalar receiver, located at the far field of a scalar transmitter, and d = z or y. Similarly, we can write $P_z^d(f) = (jk)^{-2}\partial^2 P(f)/\partial L_{Tx,d}\partial L_{Rx,z}$ and $P_y^d(f) = (jk)^{-2}\partial^2 P(f)/\partial L_{Tx,d}\partial L_{Rx,y}$, where $\partial L_{Rx,z}$ and $\partial L_{Rx,y}$ correspond to derivatives at the receive side in z and y directions, respectively. By inserting these channel representations into the definitions of channel powers, powers of the three channels $P^d(f)$, $P_z^d(f)$ and $P_y^d(f)$, d = z or y, can be written in terms of the derivatives of the pressure channel correlation $C_P = E[P_{11}(f)P_{22}^*(f)]$

$$\begin{aligned}
\Omega^d &= E[|P^d(f)|^2] = -k^{-2}\partial^2 C_P / \partial L_{Tx,d}^2 \,|_{L_{Tx,z}=L_{Tx,y}=L_{Rx,z}=L_{Rx,y}=0}, \\
\Omega_z^d &= E[|P_z^d(f)|^2] = k^{-4}\partial^4 C_P / \partial L_{Tx,d}^2 \partial L_{Rx,z}^2 \,|_{L_{Tx,z}=L_{Tx,y}=L_{Rx,z}=L_{Rx,y}=0}, \\
\Omega_y^d &= E[|P_y^d(f)|^2] = k^{-4}\partial^4 C_P / \partial L_{Tx,d}^2 \partial L_{Rx,y}^2 \,|_{L_{Tx,z}=L_{Tx,y}=L_{Rx,z}=L_{Rx,y}=0}.
\end{aligned} \quad (63)$$

Based on (20) we obtain

$$\begin{aligned}
\Omega_z^d &= \Omega^d(\Lambda_b E[\sin^2(\gamma^b)] + (1-\Lambda_b)E[\sin^2(\gamma^s)]), \\
\Omega_y^d &= \Omega^d(\Lambda_b E[\cos^2(\gamma^b)] + (1-\Lambda_b)E[\cos^2(\gamma^s)]),
\end{aligned} \quad (64)$$

where for d = z, y, we have $\Omega^z = (\Lambda_B E[\sin^2(\theta^B)] + (1-\Lambda_B)E[\sin^2(\theta^S)])$ and $\Omega^y = (\Lambda_B E[\cos^2(\theta^B)] + (1-\Lambda_B)E[\cos^2(\theta^S)])$, respectively. Using (64) it can be shown that $\Omega^d = \Omega_z^d + \Omega_y^d$.

Channel correlations between $P^d(f)$, $P_z^d(f)$ and $P_y^d(f)$ can be similarly calculated using the following relations

$$\begin{aligned}
\rho_z^d &= E[P^d(f)\{P_z^d(f)\}^*] = jk^{-3}\partial^3 C_P / \partial L_{Tx,d}^2 \partial L_{Rx,z} \,|_{L_{Tx,z}=L_{Tx,y}=L_{Rx,z}=L_{Rx,y}=0}, \\
\rho_{zy}^d &= E[P_z^d(f)\{P_y^d(f)\}^*] = k^{-4}\partial^4 C_P / \partial L_{Tx,d}^2 \partial L_{Rx,z}\partial L_{Rx,y} \,|_{L_{Tx,z}=L_{Tx,y}=L_{Rx,z}=L_{Rx,y}=0}, \\
\rho_y^d &= E[P^d(f)\{P_y^d(f)\}^*] = jk^{-3}\partial^3 C_P / \partial L_{Tx,d}^2 \partial L_{Rx,y} \,|_{L_{Tx,z}=L_{Tx,y}=L_{Rx,z}=L_{Rx,y}=0}.
\end{aligned} \quad (65)$$

For the Gaussian angular model (with small angle spreads) in shallow waters [11], we have the following Taylor series for θ^B

$$\cos(\theta^B) \approx \cos(\mu_B) - \sin(\mu_B)(\theta^B - \mu_B), \quad \sin(\theta^B) \approx \sin(\mu_B) + \cos(\mu_B)(\theta^B - \mu_B). \tag{66}$$

$$\begin{aligned}
&C_P(L_{Tx,z}, L_{Tx,y}, L_{Rx,z}, L_{Rx,y}) \\
&= [\Lambda_B \exp\{jk(L_{Tx,z}\sin(\mu_B) + L_{Tx,y}\cos(\mu_B))\}\exp\{-0.5\sigma_B^2 k^2 (L_{Tx,z}\cos(\mu_B) - L_{Tx,y}\sin(\mu_B))^2\} \\
&+(1-\Lambda_B)\exp\{jk(L_{Tx,z}\sin(\mu_S) + L_{Tx,y}\cos(\mu_S))\}\exp\{-0.5\sigma_S^2 k^2 (L_{Tx,z}\cos(\mu_S) - L_{Tx,y}\sin(\mu_S))^2\}] \\
&\times[\Lambda_b \exp\{jk(L_{Rx,z}\sin(\mu_b) + L_{Rx,y}\cos(\mu_b))\}\exp\{-0.5\sigma_b^2 k^2 (L_{Rx,z}\cos(\mu_b) - L_{Rx,y}\sin(\mu_b))^2\} \\
&+(1-\Lambda_b)\exp\{jk(L_{Rx,z}\sin(\mu_s) + L_{Rx,y}\cos(\mu_s))\}\exp\{-0.5\sigma_s^2 k^2 (L_{Rx,z}\cos(\mu_s) - L_{Rx,y}\sin(\mu_s))^2\}].
\end{aligned} \tag{67}$$

Similar relations can be obtained for the other three random variables θ^S, γ^b and γ^s. By substituting these into (20) and using the characteristic function of a zero-mean Gaussian variable $\int (2\pi\sigma^2)^{-1/2}\exp[-x^2/(2\sigma^2)]\exp(j\varsigma x)dx = \exp(-\sigma^2\varsigma^2/2)$ [40], the pressure channel correlation in (20) can be reduced to (67). For $L_{Tx,z} = L_{Tx,y} = L_{Rx,y} = 0$, i.e., a single scalar transmitter and a vertical receive dipole, (67) simplifies to (32) in [11]. Substitution of (67) into (63) and (65) results in (21) and (22).

APPENDIX IV
CLOSED-FORM EXPRESSION FOR SYMBOL ESTIMATION ERROR

For the isotropic noise model it can be shown that the noise terms in (11) are uncorrelated [10], i.e., $E[\xi_2^{(m)}(n)\{\xi_y^{(\tilde{m})}(\tilde{n})\}^*] = E[\xi_2^{(m)}(n)\{\xi_z^{(\tilde{m})}(\tilde{n})\}^*] = E[\xi_z^{(m)}(n)\{\xi_y^{(\tilde{m})}(\tilde{n})\}^*] = 0$, $\forall m$, $\tilde{m} = 1,2,3,4$ and $\forall n$, $\tilde{n} = 0, 1, \ldots, K+M-2$. Additionally, for the noise powers we have [10] $\Delta = E[|\xi_2^{(m)}(n)|^2]$, $\Delta_y = E[|\xi_y^{(m)}(n)|^2] = \Delta/2$ and $\Delta_z = E[|\xi_z^{(m)}(n)|^2] = \Delta/2$, $\forall m,n$. The noise covariance matrices can therefore be reduced to

$$\mathbf{\Sigma} = \dot{\mathbf{\Sigma}} = \begin{bmatrix} \Delta & 0 & 0 \\ 0 & \Delta/2 & 0 \\ 0 & 0 & \Delta/2 \end{bmatrix} \otimes \mathbf{I}_{K+M-1}, \tag{68}$$

where the property $\mathbf{Q}\mathbf{Q}^\dagger = \mathbf{I}_{K+M-1}$ is used and $\mathbf{I}_{K+M-1}$ is the $(K+M-1)\times(K+M-1)$ identity matrix. Now we compute the elements of the large matrix in (30). We start by the {1,1} sub-matrix, for which we have

$$\begin{aligned}
\{\dot{\mathbf{H}}^p\}^\dagger \dot{\mathbf{\Sigma}}^{-1}\dot{\mathbf{H}}^p &= \Delta^{-1}[\dot{\mathbf{H}}_7^\dagger \ \dot{\mathbf{H}}_8^\dagger \ \dot{\mathbf{H}}_9^\dagger]\left(\begin{bmatrix} 1 & 0 & 0 \\ 0 & 2 & 0 \\ 0 & 0 & 2 \end{bmatrix} \otimes \mathbf{I}_{K+M-1}\right)\begin{bmatrix} \dot{\mathbf{H}}_7 \\ \dot{\mathbf{H}}_8 \\ \dot{\mathbf{H}}_9 \end{bmatrix} \\
&= \Delta^{-1}(\dot{\mathbf{H}}_7^\dagger\dot{\mathbf{H}}_7 + 2\dot{\mathbf{H}}_8^\dagger\dot{\mathbf{H}}_8 + 2\dot{\mathbf{H}}_9^\dagger\dot{\mathbf{H}}_9) = \Delta^{-1}\mathbf{Q}^T(\mathbf{H}_7^\dagger\mathbf{H}_7 + 2\mathbf{H}_8^\dagger\mathbf{H}_8 + 2\mathbf{H}_9^\dagger\mathbf{H}_9)\mathbf{Q}^*,
\end{aligned} \tag{69}$$

$$(\{\dot{\mathbf{H}}^{y}\}^{\dagger}\dot{\boldsymbol{\Sigma}}^{-1}\dot{\mathbf{H}}^{y})^{*}=\left(-j[\dot{\mathbf{H}}_4^{T}\ \dot{\mathbf{H}}_5^{T}\ \dot{\mathbf{H}}_6^{T}]\dot{\boldsymbol{\Sigma}}^{-1}j\begin{bmatrix}\dot{\mathbf{H}}_4^{*}\\ \dot{\mathbf{H}}_5^{*}\\ \dot{\mathbf{H}}_6^{*}\end{bmatrix}\right)^{*}=\Delta^{-1}(\dot{\mathbf{H}}_4^{\dagger}\dot{\mathbf{H}}_4+2\dot{\mathbf{H}}_5^{\dagger}\dot{\mathbf{H}}_5\ +2\dot{\mathbf{H}}_6^{\dagger}\dot{\mathbf{H}}_6) \tag{70}$$
$$=\Delta^{-1}\mathbf{Q}^{T}(\mathbf{H}_4^{\dagger}\mathbf{H}_4+2\mathbf{H}_5^{\dagger}\mathbf{H}_5+2\mathbf{H}_6^{\dagger}\mathbf{H}_6)\mathbf{Q}^{*},$$

$$(\{\dot{\mathbf{H}}^{z}\}^{\dagger}\dot{\boldsymbol{\Sigma}}^{-1}\dot{\mathbf{H}}^{z})^{*}=\Delta^{-1}(\dot{\mathbf{H}}_1^{\dagger}\dot{\mathbf{H}}_1+2\dot{\mathbf{H}}_2^{\dagger}\dot{\mathbf{H}}_2+2\dot{\mathbf{H}}_3^{\dagger}\dot{\mathbf{H}}_3)=\Delta^{-1}\mathbf{Q}^{T}(\mathbf{H}_1^{\dagger}\mathbf{H}_1+2\mathbf{H}_2^{\dagger}\mathbf{H}_2+2\mathbf{H}_3^{\dagger}\mathbf{H}_3)\mathbf{Q}^{*}. \tag{71}$$

The last expressions in (69)-(71) hold true because using $\dot{\mathbf{H}}_l=\mathbf{Q}\mathbf{H}_l\mathbf{Q}^{*}$, it is straightforward to verify that $\dot{\mathbf{H}}_l^{\dagger}\dot{\mathbf{H}}_l=\mathbf{Q}^{T}\mathbf{H}_l^{\dagger}\mathbf{H}_l\mathbf{Q}^{*}, l=1,2,...,9$. Similar expressions can be obtained for {2,2} and {3,3} sub-matrices in (30). The off-diagonal sub-matrices in (30) can be shown to be **0**. As an example, for the {1,2} sub-matrix we have

$$\{\dot{\mathbf{H}}^{p}\}^{\dagger}\dot{\boldsymbol{\Sigma}}^{-1}\dot{\mathbf{H}}^{z}-(\{\dot{\mathbf{H}}^{z}\}^{\dagger}\dot{\boldsymbol{\Sigma}}^{-1}\dot{\mathbf{H}}^{p})^{*}=[\dot{\mathbf{H}}_7^{\dagger}\ \dot{\mathbf{H}}_8^{\dagger}\ \dot{\mathbf{H}}_9^{\dagger}]\dot{\boldsymbol{\Sigma}}^{-1}\begin{bmatrix}\dot{\mathbf{H}}_1^{*}\\ \dot{\mathbf{H}}_2^{*}\\ \dot{\mathbf{H}}_3^{*}\end{bmatrix}-\left([\dot{\mathbf{H}}_1^{T}\ \dot{\mathbf{H}}_2^{T}\ \dot{\mathbf{H}}_3^{T}]\dot{\boldsymbol{\Sigma}}^{-1}\begin{bmatrix}\dot{\mathbf{H}}_7\\ \dot{\mathbf{H}}_8\\ \dot{\mathbf{H}}_9\end{bmatrix}\right)^{*} \tag{72}$$
$$=\Delta^{-1}(\dot{\mathbf{H}}_7^{\dagger}\dot{\mathbf{H}}_1^{*}+2\dot{\mathbf{H}}_8^{\dagger}\dot{\mathbf{H}}_2^{*}+2\dot{\mathbf{H}}_9^{\dagger}\dot{\mathbf{H}}_3^{*}-\dot{\mathbf{H}}_1^{\dagger}\dot{\mathbf{H}}_7^{*}-2\dot{\mathbf{H}}_2^{\dagger}\dot{\mathbf{H}}_8^{*}-2\dot{\mathbf{H}}_3^{\dagger}\dot{\mathbf{H}}_9^{*})=\mathbf{0}.$$

The last identity in (72) holds true because $\dot{\mathbf{H}}_l$ is diagonal, $l=1,2,\cdots,9$, which results in $\dot{\mathbf{H}}_l^{\dagger}\dot{\mathbf{H}}_{l'}^{*}=\dot{\mathbf{H}}_{l'}^{*}\dot{\mathbf{H}}_l^{\dagger}=\dot{\mathbf{H}}_{l'}^{\dagger}\dot{\mathbf{H}}_l^{*}$. Overall, the large matrix in (30) and therefore $\boldsymbol{\mathcal{W}}$ there are block diagonal matrices. This allows the estimation error covariance matrix of the data vector $\mathbf{S}_1$ to be written as

$$\mathbf{W}=E[(\hat{\mathbf{S}}_1-\mathbf{S}_1)(\hat{\mathbf{S}}_1-\mathbf{S}_1)^{\dagger}]=E[\mathbf{Q}^{-1}(\hat{\bar{\mathbf{S}}}_1-\bar{\bar{\mathbf{S}}}_1)(\hat{\bar{\mathbf{S}}}_1-\bar{\bar{\mathbf{S}}}_1)^{\dagger}\{\mathbf{Q}^{-1}\}^{\dagger}]=E[\mathbf{Q}^{*}(\{1,1\}\text{ sub-matrix of }\boldsymbol{\mathcal{W}})\mathbf{Q}], \tag{73}$$

where we have used these properties of the **Q** matrix: $\mathbf{Q}^{-1}=\mathbf{Q}^{*}$ and $\mathbf{Q}^{T}=\mathbf{Q}$ [26]. By inserting the sum of the last equations of (69)-(71) into (73) and using (68), (31) can be obtained for the estimation error covariance matrix of the data vector $\mathbf{S}_1$. The same result holds true for $\mathbf{S}_2$ and $\mathbf{S}_3$.

APPENDIX V
DEGREES OF FREEDOM OF VECTOR AND SCALAR TRANSMITTERS

In the statistical channel model, the channel correlation has a separable Kronecker structure, as shown in (20). Therefore the vector transmitter channel correlation matrix can be written as

$$\mathbf{C}_{vector}=\begin{bmatrix}1 & \rho^{y} & \rho^{z}\\ \{\rho^{y}\}^{*} & \Omega^{y} & \{\rho^{zy}\}^{*}\\ \{\rho^{z}\}^{*} & \rho^{zy} & \Omega^{z}\end{bmatrix}. \tag{74}$$

With $P^{d}(f)=(jk)^{-1}\partial P_{22}(f)/\partial L_{Tx,d}$, $d = z$ or y, elements of this matrix can be derived as follows

$$\rho^{y}=E[P_{12}(f)\{P^{y}(f)\}^{*}]=(jk)^{-1}\partial C_P/\partial L_{Tx,y}\Big|_{L_{Tx,y}=L_{Rx,z}=L_{Rx,y}=0,L_{Tx,z}=L_{Tx}},$$
$$\rho^{z}=E[P_{12}(f)\{P^{z}(f)\}^{*}]=(jk)^{-1}\partial C_P/\partial L_{Tx,z}\Big|_{L_{Tx,y}=L_{Rx,y}=L_{Rx,z}=0,L_{Tx,z}=L_{Tx}}, \tag{75}$$
$$\rho^{zy}=E[P^{z}(f)\{P^{y}(f)\}^{*}]=-k^{-2}\partial^{2}C_P/\partial L_{Tx,z}\partial L_{Tx,y}\Big|_{L_{Tx,y}=L_{Tx,z}=L_{Rx,y}=L_{Rx,z}=0}.$$

For the system with three scalar transmitters, the transmit channel correlation matrix is given by

$$\mathbf{C}_{scalar}=\begin{bmatrix}1 & \sqrt{0.5}\rho_{12} & \sqrt{0.5}\rho_{13}\\ \sqrt{0.5}\{\rho_{12}\}^{*} & 0.5 & 0.5\rho_{23}\\ \sqrt{0.5}\{\rho_{13}\}^{*} & 0.5\{\rho_{23}\}^{*} & 0.5\end{bmatrix}, \tag{76}$$

where

$$\begin{aligned}\rho_{12}&=E[P_{12}(f)P_{22}^{*}(f)]=C_P\big|_{L_{Tx,y}=L_{Rx,y}=L_{Rx,z}=0,L_{Tx,z}=L_{Tx}},\\ \rho_{13}&=E[P_{12}(f)P_{32}^{*}(f)]=C_P\big|_{L_{Rx,y}=L_{Rx,z}=0,L_{Tx,y}=-L_{Tx},L_{Tx,z}=L_{Tx}},\\ \rho_{23}&=E[P_{22}(f)P_{32}^{*}(f)]=C_P\big|_{L_{Tx,z}=L_{Rx,y}=L_{Rx,z}=0,L_{Tx,y}=-L_{Tx}}.\end{aligned} \tag{77}$$

Using the definition of system degrees of freedom in [32] and based on the correlation function for C_P in (67), the following Taylor expansions can be obtained for channels with small angle spreads, as $\mu_B\to\pi^{-}$ and $\mu_S\to\pi^{+}$

$$\begin{aligned}\chi_{vector}&=\frac{(\mathrm{tr}[\mathbf{C}_{vector}])^2}{\mathrm{tr}[\mathbf{C}_{vector}\mathbf{C}_{vector}^{\dagger}]}\approx 1+(1+0.5k^2L_{Tx}^2)((1-\Lambda_B)\sigma_s^2+\Lambda_B\sigma_B^2)\\ &+(2+k^2L_{Tx}^2)(1-\Lambda_B)\Lambda_B(\pi-\mu_B)(\mu_S-\pi)+(1+0.5k^2L_{Tx}^2)(1-\Lambda_B)\Lambda_B[(\mu_B-\pi)^2+(\mu_S-\pi)^2],\end{aligned} \tag{78}$$

$$\begin{aligned}\chi_{scalar}&=\frac{(\mathrm{tr}[\mathbf{C}_{scalar}])^2}{\mathrm{tr}[\mathbf{C}_{scalar}\mathbf{C}_{scalar}^{\dagger}]}\approx 1+0.5k^2L_{Tx}^2((1-\Lambda_B)\sigma_S^2+\Lambda_B\sigma_B^2)\\ &+k^2L_{Tx}^2(1-\Lambda_B)\Lambda_B(\pi-\mu_B)(\mu_S-\pi)+0.5k^2L_{Tx}^2(1-\Lambda_B)\Lambda_B[(\mu_B-\pi)^2+(\mu_S-\pi)^2].\end{aligned} \tag{79}$$

In the above equations χ is the system degrees of freedom and $\mathrm{tr}[\cdot]$ is the trace operator. As shown in (33), one can verify that $\chi_{vector}-\chi_{scalar}>0$.

REFERENCES

[1] X. Zhong and B. Permkumar, "Particle filtering approaches for multiple acoustic source detection and 2-D direction of arrival estimation using a single acoustic vector sensor," *IEEE Trans. Signal Processing*, vol. 60, pp. 4719 - 4733, 2012.

[2] X. Yuan, "Estimating the DOA and the polarization of a polynomial-phase signal using a single solarized vector-sensor," *IEEE Trans. Signal Processing*, vol. 60, pp. 1270-1282, 2012.

[3] X. Guo, S. Miron, D. Brie, S. Zhu and X. Liao, "A CANDECOMP/PARAFAC perspective on uniqueness of DOA estimation using a vector sensor array ," *IEEE Trans. Signal Processing*, vol. 59, pp. 3475-3481, 2011.

[4] N. Zou and A. Nehorai, "Circular acoustic vector-sensor array for mode beamforming," *IEEE Trans. Signal Processing*, vol. 57, pp. 3041-3052, 2009.

[5] Y. I. Wu, K. T. Wong and S.K. Lau, "The acoustic vector-sensor's near-field array-manifold," *IEEE Trans. Signal Processing*, vol. 58, pp. 3946-3951, 2010.

[6] N. L. Bihan, S. Miron and J.I. Mars, "MUSIC algorithm for vector-sensors array using biquaternions," *IEEE Trans. Signal Processing*, vol. 55, pp. 4523, 2007.

[7] M. Hawkes and A. Nehorai, "Wideband source locatization using a distributed acoustic vector-sensor array," *IEEE Trans. Signal Processing*, vol. 51, pp. 1497-1491, 2003.

[8] M. Hawkes and A. Nehorai, "Acoustic vector-sensor beamforming and Capon direction estimation," *IEEE Trans. Signal Processing*, vol. 46, pp. 2291-2304, 1998.

[9] A. Nehorai and E. Paldi, "Acoustic vector-sensor array processing," *IEEE Trans. Signal Processing*, vol. 42, pp. 2481-2491, 1994.

[10] A. Abdi and H. Guo, "A new compact multichannel receiver for underwater wireless communication networks," *IEEE Trans. Wireless Commun.*, vol. 8, pp. 3326-3329, 2009.

[11] A. Abdi and H. Guo, "Signal correlation modeling in acoustic vector sensor arrays," *IEEE Trans. Signal Processing*, vol. 57, pp. 892-903, 2009.

[12] H. Guo, A. Abdi, A. Song and M. Badiey, "Delay and Doppler spreads in underwater acoustic particle velocity channels," *J. Acoust. Soc. Am.*, vol. 129, pp. 2015-2025, 2011.

[13] A. Song, A. Abdi, M. Badiey and P. Hursky, "Experimental demonstration of underwater acoustic communication by vector sensors," *IEEE J. Oceanic Eng.*, vol. 36, pp. 454 - 461, 2011.

[14] C. H. Sherman and J. L. Butler, *Transducers and Arrays for Underwater Sound*. New York: Springer, 2007.

[15] L. M. Brekhovskikh and Yu. P. Lysanov, *Fundamentals of Ocean Acoustics*. New York: Springer, 2003.

[16] A. Zielinski, Y. H. Yoon and L. Wu, "Performance analysis of digital acoustic communication in a shallow water channel," *IEEE J. Oceanic Eng.* , vol. 20, pp. 293-299, 1995.

[17] C. P. Shah, C. C. Tsimenidis, B. S. Sharif, and J. A. Neasham, "Low complexity iterative receiver design for shallow water acoustic channels," *EURASIP J. Advances in Signal Processing*, pp. 1-13, 2010.

[18] N. Richard and U. Mitra, "Sparse channel estimation for cooperative underwater communications: A structured multichannel approach," in *Proc. IEEE Int. Conf. Acoust., Speech, Signal Processing*, Las Vegas, NV, 2008, pp. 5300-5303.

[19] J. Li, J. Lu and J. Zhao, "A robust constant modulus algorithm in alpha stable noise environments," in *Proc. IEEE Int. Conf. Signal Processing*, Beijing, China, 2010, pp. 1589-1592.

[20] C. He, J. Huang and Z. Ding, "A variable-rate spread-spectrum system for underwater acoustic communications," *IEEE J. Oceanic Eng.*, vol. 34, pp. 624-633, 2009.

[21] A. G. Zajic, "Statistical modeling of MIMO mobile-to-mobile underwater channels," *IEEE Trans. Vehic. Technol.*, vol. 60, pp. 1337–1351, 2011.

[22] R. J. Urick, *Principles of Underwater Sound*. New York: McGraw-Hill, 1975.

[23] H. Xu, D. Chizhik, H. Huang and R. Valenzuela, "A generalized space-time multiple-input multiple-output (MIMO) channel model," *IEEE Trans. Wireless Commun.*, vol. 3, pp. 966-975, 2004.

[24] A. F. Molisch, *Wireless Communication*. New York: Wiley, 2005.

[25] N. Yang and M. Salehi, "A new full rate full diversity orthogonal space-time block code for three transmit antennas," in *Proc. IEEE Conf. on Inform. Science and System*, 2007, pp. 851-856.

[26] N. Al-Dhahir, "Single-carrier frequency-domain equalization for space-time block coded transmissions over frequency-selective fading channels," *IEEE Commun. Lett.*, vol.5, pp. 304-306, 2001.

[27] S. M. Kay, *Fundamentals of Statistical Signal Processing: Estimation Theory*. Englewood Cliffs, NJ: PTR Prentice-Hall, 1993.

[28] S. Ohno, "Performance of single-carrier block transmissions over multipath fading channels with linear equalization," *IEEE Trans. Signal Processing*, vol. 54, pp. 3678 – 3687, 2006.

[29] C. Tepedelenlioglu and Q. Ma, "On the performance of linear equalizers for block transmission systems," in *Proc. IEEE Globol Telecommun. Conf.*, St. Louis, MO, 2005, pp. 3892-3896.

[30] G. D. Durgin, *Space-Time Wireless Channels*. Upper Saddle River, NJ: Prentice-Hall PTR, 2003.

[31] R. Janaswamy, *Radiowave Propagation and Smart Antennas for Wireless Communications*. Boston: Kluwer, 2001.

[32] T. Muharemovic, A. Sabharwal and B. Aazhang, "Antenna packing in low-power systems: Communication limits and array design," *IEEE Trans. Inform. Theory*, vol. 54, pp. 429-440, 2008.

[33] C. Chen and A. Abdi, "A vector sensor receiver for chirp modulation in underwater acoustic particle velocity channels," in *Proc. Conf. on Underwater Communications: Channel Modelling and Validation*, Sestri Levante, Italy, 2012, pp. 1-8.

[34] E. Kinsler and A. R. Frey, *Fundamentals of Acoustics*, 2nd ed., New York: Wiley, 1962.

[35] B. A. Cray, V. M. Evora and A. H. Nuttall, "Highly directional acoustic receivers," *J. Acoust. Soc. Am.*, vol. 113, pp. 1526-1532, 2003.

[36] C. Chen, *Transceiver Design for Underwater Communication via Vector Fields*. PhD Thesis, New Jersey Institute of Technology, Newark, NJ, 2012.

[37] T. S. Rappaport, *Wireless Communications: Principles and Practice*, 2nd ed., Upper Saddle River, NJ: PTR Prentice-Hall, 2002.

[38] A. Abdi, H. Hashemi and S. Nader-Esfahani, "On the PDF of the sum of random vectors," *IEEE Trans. Commun.*, vol. 48, pp. 7-12, 2000.

[39] A. Abdi, "On the utility of Laguerre series for the envelope PDF in multipath fading channels," *IEEE Trans. Inform. Theory*, vol. 55, pp. 5652-5660, 2009.

[40] A. Papoulis, *Probability, Random Variables, and Stochastic Processes*, 3rd ed., Singapore: McGraw-Hill, 1991.

Chen Chen received the Ph.D. degree in electrical engineering from New Jersey Institute of Technology (NJIT), Newark. She received her B.S. and M.S. degrees both from Southeast University, Nanjing, China. She is now affiliated with Litepoint Corp., Sunnyvale, CA.

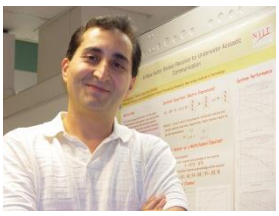

Ali Abdi (S'98, M'01, SM'06) received the Ph.D. degree in electrical engineering from the University of Minnesota, Minneapolis. He joined the Department of Electrical and Computer Engineering of New Jersey Institute of Technology (NJIT), Newark, where he is currently an Associate Professor. His current

research interests include characterization and estimation of wireless channels, digital communication in underwater and terrestrial channels, acoustic signal processing, blind modulation recognition, systems biology and molecular networks. Dr. Abdi was an Associate Editor for IEEE Transactions on Vehicular Technology from 2002 to 2007. Dr. Abdi has received 2006 NJIT Excellence in Teaching Award, in the category of Excellence in Team, Interdepartmental, Multidisciplinary, or Non-Traditional Teaching. He has also received New Jersey Inventors Hall of Fame (NJIHoF) Innovators Award and IEEE Region 1 Award, for his work on underwater acoustic communication.